International Journal of Biological Macromolecules 310 (2025) 143314

Contents lists available at ScienceDirect

International Journal of Biological Macromolecules

journal homepage: www.elsevier.com/locate/ijbiomac

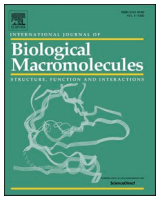

Oxygen-generating and antibacterial xanthan gum/PLA aerogels loaded with dexamethasone for potential wound healing

Nika Atelšek Hozjan [a], Gabrijela Horvat [a], Matjaž Finšgar [a], Ana Iglesias-Mejuto [b], Inés Ardao Palacios [c], Carlos A. García-González [b], Željko Knez [a], Zoran Novak [a,*]

[a] Faculty of Chemistry and Chemical Engineering, University of Maribor, Smetanova ul.17, SI-2000 Maribor, Slovenia
[b] AerogelsLab, I+D Farma Group (GI-1645), Department of Pharmacology, Pharmacy and Pharmaceutical Technology, Faculty of Pharmacy, iMATUS and Health Research Institute of Santiago de Compostela (IDIS), Universidade de Santiago de Compostela, 15782 Santiago de Compostela, Spain
[c] Centro Singular de Investigaci.n en Medicina Molecular y Enfermedades Crónicas (CiMUS), Universidade de Santiago de Compostela, 15782 Santiago de Compostela, Spain

ARTICLE INFO

Keywords:
Aerogel
Wound healing
Xanthan gum

ABSTRACT

Chronic wounds do not heal within a reasonable time frame due to hypoxia and bacterial inflammation, creating an urgent need for advanced biomaterials to address these challenges. In this study, oxygen-generating, antibacterial xanthan gum-polylactic acid (XA/PLA) aerogels loaded with dexamethasone were developed for the first time for potential wound healing applications. The aerogels contained sodium percarbonate and calcium peroxide as oxygen-releasing agents, providing sustained oxygen release for up to 48 h. The aerogels had a highly porous structure with a high specific surface area (up to 396 ± 8 m^2/g) and revealed high liquid absorption capacity in simulated body fluid, absorbing up to 67 times their original weight and remaining stable for 72 h. The *in vitro* release tests showed controlled profiles of dexamethasone over 24 h. The antibacterial tests demonstrated strong antibacterial activity against *Escherichia coli* (an up to 15.92 mm inhibition zone diameter) and *Staphylococcus aureus* (up to a 31.07 mm inhibition zone diameter). The *in vitro* biocompatibility assays revealed good cytocompatibility with mouse fibroblast cells (NIH/3T3), with a cell viability of >90%. Hemocompatibility tests showed no hemolytic activity with human blood (lysis rate <2%). Overall, these results emphasise the versatility of the XA/PLA aerogels and their potential for the treatment of chronic wounds.

1. Introduction

Chronic wounds are complex and serious medical conditions affecting millions of individuals worldwide, placing a significant burden on healthcare systems in terms of both resources and costs [1,2]. These wounds are usually characterised by chronic inflammation, bacterial colonisation, and the formation of drug-resistant microbial biofilms [1,3]. Another critical factor in the pathogenesis of chronic wounds is hypoxia, defined as inadequate oxygen levels at the wound site, which impede the healing process severely [4,5]. Addressing these challenges necessitates the development of novel and versatile wound dressing materials capable of eliminating bacteria, delivering drugs, and oxygenating the wound site simultaneously.

Conventional dressings, such as gauze or bandages, provide primarily physical protection but require frequent change, which can lead to dehydration of the wound and disruption to the healing process [6,7]. In contrast, advanced dressings like hydrogels and films create a moist wound environment that promotes healing; however, they are associated with considerable limitations. For instance, hydrogels are unable to absorb substantial amounts of wound exudate and exhibit poor stability at room temperature. Additionally, their low gas permeability prevents oxygen diffusion to the wound site, which is crucial for tissue regeneration. While hydrogels can incorporate drugs or therapeutic agents, their release profiles are often uncontrolled, limiting their ability to provide sustained or targeted delivery. Similarly, films provide a protective barrier against external contaminants, but tend to adhere to the wound, causing discomfort upon removal. Their inability to absorb large amounts of wound exudate limits their application to wounds with low exudate production [8]. In addition, films are generally not customisable, making it difficult to optimise their properties for specific wound types or stages of healing [9–12].

Aerogels, with their exceptional properties, are emerging as

* Corresponding author.
E-mail address: zoran.novak@um.si (Z. Novak).

https://doi.org/10.1016/j.ijbiomac.2025.143314
Received 2 December 2024; Received in revised form 7 April 2025; Accepted 16 April 2025
Available online 19 April 2025

promising materials for wound healing applications [13,14]. Unlike hydrogels and films, aerogels have highly porous structures that enable superior liquid absorption, allowing them to absorb large amounts of wound exudate [15–18]. Their substantially larger specific surface area allows the incorporation of bioactive compounds, such as antibiotics or anti-inflammatory drugs, enabling a controlled and sustained release to support the healing process more effectively [19]. In recent years, aerogels produced from polysaccharides and biopolymers (commonly referred to as bioaerogels) have gained recognition as ideal raw materials for producing wound dressings, due to their biocompatibility, biodegradability and non-toxicity. Notably, recent studies have demonstrated the efficacy of bioaerogels based on alginate [20], chitosan [21] and pectin [9] in promoting wound healing by maintaining moisture, exhibiting excellent fluid absorption and delivering bioactive components in a controlled manner. Despite advances in commercial wound dressings, many continue to face substantial limitations, such as inadequate moisture management and limited antimicrobial or drug-release capabilities. A brief comparison with aerogels is provided in the Supplementary material (Table S1).

Xanthan gum (XA) is a biocompatible and non-toxic polysaccharide [22,23] that has not yet received significant attention in wound dressing development [10]. XA's hydrophilic nature enables it to bind water and absorb large quantities of liquids, thereby creating and maintaining a moist environment around the wound while absorbing wound exudate efficiently [4,10,12]. In contrast, polylactic acid (PLA), a widely used biopolymer in biomedical applications, is known for its biodegradability and biocompatibility, making it tolerated well by the human body [24–26]. PLA also provides structural support to the final material, and enables controlled drug release [27], properties that are particularly beneficial in wound healing [28,29]. The combination of XA and PLA in aerogels can improve the mechanical stability, moisture retention, and biocompatibility of the material synergistically. Additionally, this unique polymer combination enables the incorporation of drugs and oxygen-generating agents, which are advantageous in the treatment of chronic wounds. The dual functionality of XA and PLA, with their complementary properties, makes them ideal candidates for the development of advanced wound healing materials.

An adequate oxygen supply is essential in hypoxic wounds for cellular survival and function [2,30]. Oxygen serves as the terminal electron acceptor in the mitochondrial electron transport chain and facilitates the generation of adenosine triphosphate (ATP), which is vital for cellular processes [31]. Moreover, oxygen fuels cellular respiration, which is critical for tissue repair [32,33]. It is also crucial for collagen synthesis, angiogenesis and epithelial cell migration – key processes involved in the various phases of wound healing [30,34,35]. To address the challenge of oxygen delivery in hypoxic wounds, several oxygen-releasing materials have been developed to promote wound healing by providing a continuous oxygen supply [34,35]. These materials often include solid oxygen-generating agents, such as calcium peroxide (CPO), sodium percarbonate (SPO) and magnesium peroxide (MPO) [30]. Among these, MPO produces the least oxygen, due to its poor solubility. Additionally, its commercial purity is much lower compared to that of SPO and CPO [35]. Upon exposure to a moist environment, these peroxides decompose into their corresponding hydroxides and hydrogen peroxide (H_2O_2). The H_2O_2 then decomposes further into oxygen and water. While this reaction provides an adequate oxygen supply, it also generates substantial amounts of cytotoxic reactive oxygen species (ROS). To mitigate this issue, researchers combine peroxides with catalase, an enzyme that converts H_2O_2 efficiently into oxygen and water, thereby reducing ROS production and enhancing the safety of these oxygen-generating systems [36,37].

Dexamethasone (DEX), an anti-inflammatory corticosteroid [38], is used frequently in tissue engineering as a component of scaffolds [39,40] and hydrogels [41]. It has been successfully used to support growth, proliferation, and osteogenic differentiation of stem cells as well as to reduce inflammation and promote tissue regeneration [38,42]. The mechanism of the action of DEX involves the suppression of pro-inflammatory gene transcription and the enhancement of anti-inflammatory processes [38,43]. By modulating these signalling pathways, the drug reduces inflammation and immune system activity effectively [38], making it particularly valuable for the treatment of various inflammatory conditions. However, the effect of DEX on wound healing can vary, depending on the context and specific characteristics of the wound [38,42]. Therefore, it is crucial to administer the drug in controlled, small doses over a short period, to maximise its therapeutic benefits and minimise potential side effects [38].

This study aimed to develop novel hybrid XA/PLA aerogels with multiple beneficial properties that have the potential to support wound healing. The main objective was to create a material with enhanced characteristics for wound care, by incorporating oxygen-generating agents (SPO and CPO) and the model anti-inflammatory drug DEX into the XA/PLA aerogels. To achieve this, affordable and biodegradable polymers were used without any chemical crosslinkers or toxic substances. Two aerogel formulations with different compositions were synthesised by the sol-gel process and supercritical drying, as illustrated in Scheme 1. The Oxygen-generating compounds (SPO and CPO) were incorporated, and the amount of gas released was measured. The aerogels were impregnated with DEX, and its release profiles were evaluated *in vitro* in simulated body fluid (SBF) over 24 h. To determine the drug release mechanism, the release data were fitted with zero-order, first-order, Higuchi and Korsmeyer-Peppas kinetic models. The physical and chemical properties of the XA/PLA aerogels were characterised comprehensively using advanced analytical techniques, including attenuated total reflection Fourier transform infrared spectroscopy (ATR-FTIR), scanning electron microscopy (SEM), and time-of-flight secondary ion mass spectrometry (ToF-SIMS). Finally, the antibacterial activity of the hybrid aerogels was assessed, and biocompatibility tests were conducted to evaluate their suitability for potential wound healing applications.

2. Materials and methods

2.1. Materials

The following chemicals were used as received: Xanthan gum from *Xanthomonas campestris* (viscosity: 930 (cps) in a 1% H_2O solution, CAS number: 11138–66-2, LOT number: #SLBN1080V), catalase from bovine liver (2000–5000 U/mg protein), Trizma® base (primary standard and buffer, ≥99,9% purity) were purchased from Sigma-Aldrich (St. Louis, USA). Polylactic acid (molecular weight: 230000 g/mol, granular, 3–5 mm nominal granule size, CAT: GF45989881-1EA) was obtained from Goodfellow (Cambridge, U.K.). Ethyl lactate ((*S*)-(−)-ethyl lactate for synthesis), sodium hydrogen carbonate for analysis (ACS reagent) and sodium sulphate (ACS reagent, ≥99,0% purity), were acquired from Merck KGaA (Darmstadt, Germany). Sodium percarbonate (available H_2O_2 20–30%), calcium peroxide (75%, -200 mesh), calcium chloride dihydrate (ACS reagent), sodium chloride (≥99,8% purity) and anhydrous magnesium chloride (≥98% purity) were purchased from Sigma-Aldrich (Darmstadt, Germany). Potassium chloride (≥99,5% purity) and hydrochloric acid (≥99,0%) were obtained from Honeywell (Seelze, Germany). Dexamethasone (>99% purity) was acquired from Tokyo Chemical Industry Co., Ltd. (Tokyo, Japan). Anhydrous potassium hydrogen phosphate (≥98% purity) was acquired from Kemika (Zagreb, Croatia). Absolute anhydrous ethanol for analysis (ACS reagent, ≥99.5% purity) was purchased from Carlo Erba (Milan, Italy). Ultra-pure water (18.2 MΩ cm at 25 °C) produced by the Milli-Q® system (EMD Millipore Corporation, USA) was used in all the experiments.

The acetate and pyruvate content of the XA was determined by proton nuclear magnetic resonance (^{1}H NMR) at 80 °C using sodium acetate (ACS reagent, >99% purity, Honeywell Fluka™, Germany) as a standard according to the previously described method [44]. The values for the acetate and pyruvate content were 0.567 and 0.513 per side

Scheme 1. Schematic of the hybrid XA/PLA-CSD aerogel synthesis process.

chain of XA, respectively. Detailed information on the sample preparation and characterisation procedures are in the Supplementary material (Section S2).

2.2. Methods

2.2.1. Preparation of hybrid alcogels with active ingredients (XA/PLA–CSD)

The preparation of hybrid XA/PLA-CSD aerogels included a sol-gel reaction followed by supercritical drying, as illustrated in Scheme 1. The acronym CSD represents C for catalase and CPO, S for SPO and D for DEX.

The alcogels were synthesised by preparing a 4% (w/v) aqueous XA solution. First, the XA was added to ultrapure water slowly while stirring (400 rpm) to prevent the formation of non-dispersed lumps. The solution was mixed for 1 h at room temperature (25 °C) until fully dissolved. Then, a 0.01 mg/mL enzyme catalase solution was prepared in ultrapure water, and an 8% (v/v) solution was added to the XA solution. Simultaneously, the PLA was added to ethyl lactate and mixed at 120–130 °C until completely dissolved (approximately 2 h) to achieve final concentrations of 2% (w/v) and 4% (w/v). Then, 4% (w/v) SPO and 4% (w/v) CPO were added to the PLA solution. Immediately afterwards, the XA solution was mixed with the PLA solution under constant stirring (30 s) and heating (55 °C). The resulting mixture was then poured into a Petri dish, and absolute ethanol was added to stop the initial oxygen production and initiate the gelation process. Afterwards, a 2.5 mg/mL DEX solution in absolute ethanol was prepared (50 mg of DEX in 20 mL of ethanol). DEX is highly soluble in ethanol and poorly soluble in non-polar solvents, such as carbon dioxide (CO_2), which was, later, used for the drying step [45]. Once gelation was complete, the initial ethanol was replaced with a DEX-ethanol solution. The gels were stored in the solution for 24 h to ensure complete diffusion of the DEX throughout the material. Finally, the XA/PLA-CSD alcogels were dried supercritically. Two different ratios of XA/PLA were used, as summarised in Table 1.

2.2.2. Preparation of reference hybrid alcogels (XA/PLA)

Reference hybrid aerogels were prepared for comparison with the XA/PLA-CSD aerogels. An aqueous solution of 4% (w/v) XA was prepared by adding XA powder to ultrapure water slowly with constant stirring (400 rpm) at 25 °C. The PLA was mixed in ethyl lactate at 120–130 °C for 2 h until the final concentrations of 2% (w/v) and 4% (w/v) were achieved. After homogenisation of the starting solutions, they were mixed under heating (55 °C). The resulting mixture was then removed from the heater and poured into a Petri dish to form a gel. Gelation was accelerated further by adding the absolute ethanol, which removed the water and ethyl lactate from the original mixture. After 2 h, the ethanol was replaced with fresh absolute ethanol, and the alcogels were stored in this solution overnight until supercritical drying.

2.2.3. Supercritical CO_2 drying

The prepared alcogels were dried using supercritical CO_2 to preserve their original structures. A supercritical extraction instrument (UHDE GmbH, Dortmund, Germany) was used for the drying process. A 500 mL autoclave was filled with absolute ethanol, and the XA/PLA–CSD or XA/PLA alcogels were immersed. The system was pre-heated to 42 °C and pressurised to 120 bars. Ethanol extraction was carried out for 6 h at a CO_2 flow rate of approximately 200 L/h. The system was then depressurised slowly and cooled to room temperature.

2.2.4. N_2 adsorption-desorption analysis

The Brunauer-Emmett-Teller (BET) method was used to determine the specific surface area (m^2/g) of the XA/PLA-CSD and XA/PLA aerogels during the N_2 adsorption-desorption analysis. The corresponding adsorption-desorption curves were plotted, and the pore size

Table 1
Composition of hybrid XA/PLA aerogels and N_2 adsorption–desorption analysis results.

Sample	XA (g)	PLA (g)	EL (g)	H_2O (g)	DEX (mg)	CPO (g)	SPO (g)	Catalase (mg)	S_{BET} (m^2/g)	Pore size (nm)
XA/PLA1	0.5	1.0	25.0	12.5	/	/	/	/	342 ± 7	18
XA/PLA2	1.0	0.5	25.0	25.0	/	/	/	/	396 ± 8	16
XA/PLA1–CSD	0.5	1.0	25.0	12.5	50.0	1.0	1.0	1.0	2	27
XA/PLA2–CSD	1.0	0.5	25.0	25.0	50.0	1.0	1.0	1.0	2	28

XA: xanthan gum, PLA: polylactic acid, CSD: catalase, calcium peroxide, sodium percarbonate, dexamethasone.

distribution was determined using the Barrett-Joyner-Halenda (BJH) method. Prior to analysis, the aerogels were degassed for 10 h at 70 °C under vacuum until a stable pressure of 10 μg Hg was reached. Subsequently, the measurements were conducted at −196 °C using an ASAP 2020 MP instrument (Micromeritics Instrument, Norcross, GA, USA).

2.2.5. Thermal analysis

Thermal analysis was used to evaluate the thermal stability of all synthesised aerogels using differential scanning calorimetry (DSC) and thermogravimetric analysis (TGA). Both measurements were performed simultaneously with a TGA/DSC 1 instrument (Mettler Toledo AG (MTANA), Zürich, Switzerland). Approximately 10 μg of the aerogel sample was placed into a 100 μL aluminium crucible alongside an empty aluminium crucible, which served as a reference. The analysis was performed under an N_2 atmosphere, with the temperature increasing from 30 °C to 600 °C at a rate of 10 °C/min.

2.2.6. ATR-FTIR

The presence of functional groups and the structure of the molecules in the hybrid XA/PLA–CSD and reference XA/PLA aerogels were investigated using ATR-FTIR. The measurements were performed with an IRAffinity-1S instrument (Shimadzu, Japan). The background spectra were compensated first, followed by the recording of the spectra of the aerogels at wavenumbers in the range of 400–4000 cm^{-1}.

2.2.7. SEM analysis

The morphology of the final aerogels was analysed using a JSM-IT800 Schottky instrument (JEOL, Tokyo, Japan). Prior to analysis, the aerogels were cut into small pieces. Since aerogels are nonconductive, they were coated with a thin layer of gold. After preparation, the aerogels were placed on an aluminium aerogel holder. The measurements were performed at two different voltages: 1.0 kV and 2.1 kV. The lower voltage of 1.0 kV was used for high-resolution imaging, while the higher voltage of 2.1 kV was used to achieve stronger signals for more detailed imaging.

2.2.8. ToF-SIMS analysis

The ToF-SIMS measurements were carried out using an M6 device (IONTOF, Münster, Germany). The setup utilised a 30 keV Bi_3^+ primary ion beam at a target current of 0.6 pA, while the charge neutralisation remained active, and a surface potential of 160 eV was applied during the experiments. The aerogel surface was sputtered with an Ar_{1900}^+ gas cluster ion beam (GCIB) to generate three-dimensional profiles. The sputtering was conducted at an accelerating voltage of 2.5 keV and a beam current of 50 pA over an area of 500 × 500 μm. The subsequent analyses focused on a 300 × 300 μm section at the centre of the sputtered area. The ToF-SIMS measured data were calibrated using known peaks at specific mass–charge ratios (*m/z*), *i.e.*, C^- at *m/z* 12.00, CH^- at *m/z* 13.01, C_2^- at *m/z* 24.00, C_2H^- at *m/z* 25.01, C_3^- at *m/z* 36.00, C_4^- at *m/z* 48.00, C_5H^- at *m/z* 61.01 in negative polarity, and $C_2H_3^+$ at *m/z* 27.02. $C_3H_5^+$ at *m/z* 41.04, $C_4H_5^+$ at *m/z* 53.04, and $C_4H_7^+$ at *m/z* 55.05 were in positive polarity.

2.2.9. Swelling and stability

The changes in the aerogel mass due to liquid uptake and their durability were measured by swelling and stability tests with a gravimetric method on a 708-DS Dissolution System (Agilent Technologies, California, USA). Initially, the SBF medium was prepared according to the previously described protocol [46], with ion concentrations of 142.0 mM Na^+, 5.0 mM K^+, 1.5 mM Mg^{2+}, 2.5 mM Ca^{2+}, 148.8 mM Cl^-, 4.2 mM HCO_3^-, 1.0 mM HPO_4^{2-} and 0.5 mM SO_4^{2-}. The pH of the SBF was adjusted to 7.40 at 36.5 °C with 1 M HCl. The dry XA/PLA aerogels (0,1 g) were then placed in cylindrical metal baskets and pre-weighed to obtain their initial dry mass (w_0). They were then attached to the apparatus and immersed in pre-heated containers with 600 mL of SBF for 72 h. The temperature was set to 37.5 °C, and the stirring speed was 50 rpm. The aerogels were removed from the containers at various time intervals: 15 min, 30 min, 45 min, 1 h, 2 h, 3 h, 4 h, 5 h, 6 h, 24 h, 48 h, and 72 h. Any excess water remaining on the basket was dabbed carefully with a paper towel. After weighing the aerogels (w_1), they were returned to the SBF. The percentage of swelling degree at each time interval was calculated using the following Eq. (1):

$$\text{Swelling degree} = \left(\frac{w_1 - w_0}{w_0}\right) \cdot 100\% \quad (1)$$

where w_1 and w_0 represent the weights of the wet and dry aerogels (g), respectively.

2.2.10. Oxygen release

The amount of oxygen released from XA/PLA-CSD aerogels was measured with the standard water displacement method. First, an SBF solution was prepared as described in Section 2.2.9. Then, approximately 10 mg of the aerogel was added to a 50 mL syringe (Chirana T. Injecta, A.S., Stará Turá, Slovakia) pre-filled with 30 mL of SBF. The syringe was fitted with a tube, and the other side was inserted into a volumetric cylinder filled with water. The amount of water displaced from the volumetric cylinder was measured at pre-determined time points up to 48 h, and was directly proportional to the amount of oxygen produced.

2.2.11. In vitro drug release

The *in vitro* drug release of DEX from XA/PLA-CSD aerogels was evaluated using the dissolution method. First, the SBF was prepared as described in Section 2.2.9.

A calibration curve was generated to quantify the released DEX. A stock solution (50 μg/mL) was prepared by dissolving 5 mg of DEX in 100 mL of SBF. This solution was then diluted to obtain final concentrations of 5, 10, 20, 30, and 40 μg/mL. The absorbance of each solution was measured at 242.5 nm using a Cary-100 UV–Vis spectrophotometer (Agilent Technologies, California, USA) [47]. The resulting calibration curve is provided in the Supplementary material (Fig. S3). The concentration of DEX released from the aerogels was calculated based on the measured absorbance values.

The dissolution study was performed using a 708 DS Dissolution System (Agilent Technologies, California, USA). Two containers, each filled with 600 mL of the SBF, were immersed in the water bath maintained at 37 ± 0.5 °C to simulate the average human body temperature. The stirring speed was set to 20 rpm and held constant throughout the experiment. The dry aerogels (50 mg) were placed in hollow metal baskets and submerged in the SBF once the temperature had stabilised. Samples were collected at 10 time points (15 min, 30 min, and 1, 2, 4, 5, 6, 8, 18, and 24 h). At each point, 1 mL of SBF was collected, filtered and

analysed using UV–Vis spectrophotometry at 242.5 nm. To maintain a constant volume, an equal amount (1 mL) of fresh SBF medium was added to the containers immediately.

All the tests were performed in triplicate, and the results are reported as mean ± standard deviation. The calibration curve was used to determine the mass concentration of released DEX, and the cumulative drug release was calculated using Eq. (2):

$$\text{Cumulative drug release} = \text{Q} = \frac{c_n \times V_0 + V_i \times \sum c_i}{m(\text{t})} \cdot 100\% \quad (2)$$

where Q represents the cumulative drug release (%), c_n is the mass concentration of DEX released at time 't' (mg/mL), V_0 is the total volume of the SBF (mL), V_i is the volume of SBF removed at each time point 't' (mL), c_i is the concentration of DEX in the removed SBF sample at each time point (mg/mL), and $m_{(t)}$ is the total amount of DEX in the aerogel sample (mg).

2.2.12. Drug loading

The impregnation of the DEX was performed with solvent exchange, as described in Section 2.2.1. To determine the DEX drug loading capacity (%), the aerogel samples (50 mg) were immersed in SBF (200 mL) and kept under constant stirring (500 rpm) until they degraded completely. The resulting solution was filtered and analysed using a Cary-100 UV–Vis spectrophotometer (Agilent Technologies, California, USA) at 242.5 nm. All the tests were performed in triplicate, and the results are reported as mean ± standard deviation. The drug loading was calculated based on the total drug released after the complete degradation of the aerogel sample in the SBF medium, following the equation below:

$$\text{Drug loading capacity} = \frac{m_t}{m_{\text{AER}}} \cdot 100\% \quad (3)$$

where m_t is the mass of DEX after complete degradation of the aerogel samples (mg), measured with the UV–Vis, and m_{AER} is the total mass of aerogel samples used for the measurement (mg). The mass of DEX was determined from the calibration curve in SBF, which was obtained and validated in the 0.005–0.05 mg/mL range ($R^2 = 0.9997$) (see Supplementary material, section S3).

2.2.13. Drug release kinetics

The drug release profiles of DEX were fitted to different mathematical models to evaluate the release kinetics and release mechanisms. The release data were plotted according to each kinetic model, and the correlation coefficient (R^2) was calculated to determine the accuracy of each model. The model with the highest R^2 value described the drug release of the XA/PLA–CSD aerogels best.

2.2.13.1. Zero-order. Zero-order drug release refers to drug release kinetics in which the drug is released at a constant rate, independent of its concentration. This model is particularly relevant for controlled-release systems, where sustained drug release is desired [48]. The mathematical expression for zero-order release is described by:

$$Q_{(t)} = Q_{(0)} + k_0 \cdot \text{t} \quad (4)$$

where $Q_{(t)}$ is the amount of the drug released at time 't', $Q_{(0)}$ is the initial amount of the drug in the sample, and k_0 is the zero-order constant.

2.2.13.2. First-order. First-order release describes the drug release kinetics, where the release rate is proportional to the remaining drug concentration in the sample. This model leads to a constant release over time, and the rate depends only on the initial drug concentration [49]. The first-order release model is expressed as follows:

$$Q_{(t)} = 1 - exp(-k_1 \cdot t) \quad (5)$$

where $(1 - Q_{(t)})$ represents the remaining fraction of the drug at the time 't' in the system, and k_1 is the first-order constant.

2.2.13.3. Higuchi model. The Higuchi model describes the drug release kinetics from a matrix system, usually a polymer, assuming a diffusion-controlled mechanism. It is based on Fick's law of diffusion and considers that drug release occurs through a homogeneous matrix, where the initial drug concentration is much higher than its solubility in the surrounding medium [50]. The Higuchi release model is represented mathematically as:

$$Q_{(t)} = k_H \cdot t^{1/2} \quad (6)$$

where $Q_{(t)}$ is the amount of drug released at time 't' and k_H is the Higuchi release rate constant.

2.2.13.4. Korsmeyer-Peppas model. The Korsmeyer-Peppas model explains the drug release kinetics from polymer systems when the release mechanism is not well-defined or involves multiple processes. It explains the exponential relationship between release and time, enabling the determination of the release exponent (n), which indicates the release mechanism. Depending on the value of n, release from cylindrical forms can follow Fickian diffusion ($n < 0.45$), non-Fickian (anomalous) transport ($0.45 < n < 0.89$), or Case-II transport ($n = 0.89$) [49]. This model applies only to the first 60% of cumulative drug release ($Q_{(t)} < 60\%$), and is expressed as follows:

$$Q_{(t)} = \frac{M_{(\text{t})}}{M_{\text{tot}}} = k_{\text{KP}} \cdot t^n \quad (7)$$

where $Q_{(t)}$ is the cumulative drug release (%), M_t is the amount of the drug released at time 't', M_{tot} is the total amount of the loaded drug, k_{KP} is the Korsmeyer-Peppas release rate constant, and n is the exponent of the release related to the drug release mechanism.

2.2.14. Antibacterial activity

The antibacterial activity of the XA/PLA-CSD aerogels was evaluated using the agar diffusion assays, which ensures direct contact of the material with the bacterial strains [51]. The experiments were performed following the Clinical and Laboratory Standards Institute (CLSI) guidelines [52]. The aerogels were tested against two common wound infection pathogens: the Gram-negative bacteria *Escherichia coli* (ATCC 25922) and the Gram-positive bacteria *Staphylococcus aureus* (ATCC 29213) [53].

The bacterial suspensions were prepared at a concentration of 0.5 McFarland (1.5×10^8 CFU/mL) in a sterile 0.9% (w/v) NaCl solution, and the agar plates were inoculated with the suspensions. The XA/PLA-CSD aerogels were cut into small pieces (50 mg), sterilised under UV light and placed on the inoculated agar plates. The plates were then labelled and incubated for 48 h at the optimum temperature for microorganism growth ($T = 35 \pm 1$ °C [52]). The antibacterial activity of the aerogels was determined by measuring the diameter of the zones of inhibition (ZOI). All the tests were performed in duplicate, and the results are reported as mean value ± standard deviation.

2.2.15. Cell viability

The viability of mouse embryo fibroblasts (NIH/3T3) was studied after 24 and 72 h of contact with 5 mg of each XA/PLA-CSD aerogel formulation, corresponding to a concentration of 8.33 mg/mL. A total of 12,000 cells/cm^2 were seeded in 24-well plates with 600 μL of Dulbecco's modified Eagle's growth medium supplemented with 10% bovine calf serum, 100 U/mL penicillin, and 100 g/mL streptomycin. The cells were incubated at 37 °C in a humidified atmosphere enriched with 5% CO_2. The aerogels were UV-sterilised for 30 min before cell testing and placed immediately in the culture inserts in contact with the cells. The cells without aerogels were incubated under the same

conditions and served as controls. After 24 and 72 h of culture, the aerogels were removed, the growth medium was aspirated, and 100 μL of 44 μM resazurin in the fresh growth medium was added to each well. The transformation of resazurin into resorufin by metabolically active cells was used to assess the cytocompatibility of the formulations. After 3 h of incubation under the same conditions, the fluorescence (excitation wavelength: 544 nm; emission wavelength: 590 nm) was measured in a microplate reader (Infinite® M200, Tecan Group Ltd., Männedorf, Switzerland). All the tests were performed in triplicate and the results are reported as mean value ± standard deviation.

2.2.16. Hemolytic activity

The hemolytic activity of the XA/PLA-CSD aerogels was studied with human blood (Galician Transfusion Center, Spain) obtained according to the Declaration of Helsinki [54]. The fresh human blood was diluted to 3% (v/v) in a 0.9% (w/v) NaCl solution, and 5 mg of the aerogels were incubated with 1 mL of diluted blood in Eppendorf tubes. Positive controls were prepared for hemolysis by placing 100 μL of 4% (v/v) Triton X-100 in contact with 1 mL of diluted blood, while negative controls were prepared by mixing 100 μL of phosphate–buffered saline (PBS, pH 7.4) with 1 mL of diluted blood. The XA/PLA-CSD samples were incubated at 37 °C and 100 rpm for 60 min, followed by centrifugation at 10,000 ×*g* for 10 min (Sigma 2-16P, Sigma Laboratory Centrifuges, Osterode am Harz, Germany). Afterwards, 150 μL of the supernatant was transferred to a 96-well plate, and the absorbance of the hemoglobin was measured at λ = 540 nm (FLUOStar Optima, BMG Labtech, Ortenberg, Germany). All the tests were performed in triplicate, and the results are reported as mean value ± standard deviation. Eq. (7) was used to calculate the percentage of hemolysis:

$$\text{Hemolysis} = \frac{A_{bss} - A_{bsn}}{A_{bsp} - A_{bsn}} \cdot 100\% \quad (8)$$

where A_{bss} is the absorbance of the aerogels, A_{bsn} is the negative control absorbance (0% hemolysis), and A_{bsp} is the positive control absorbance (100% hemolysis).

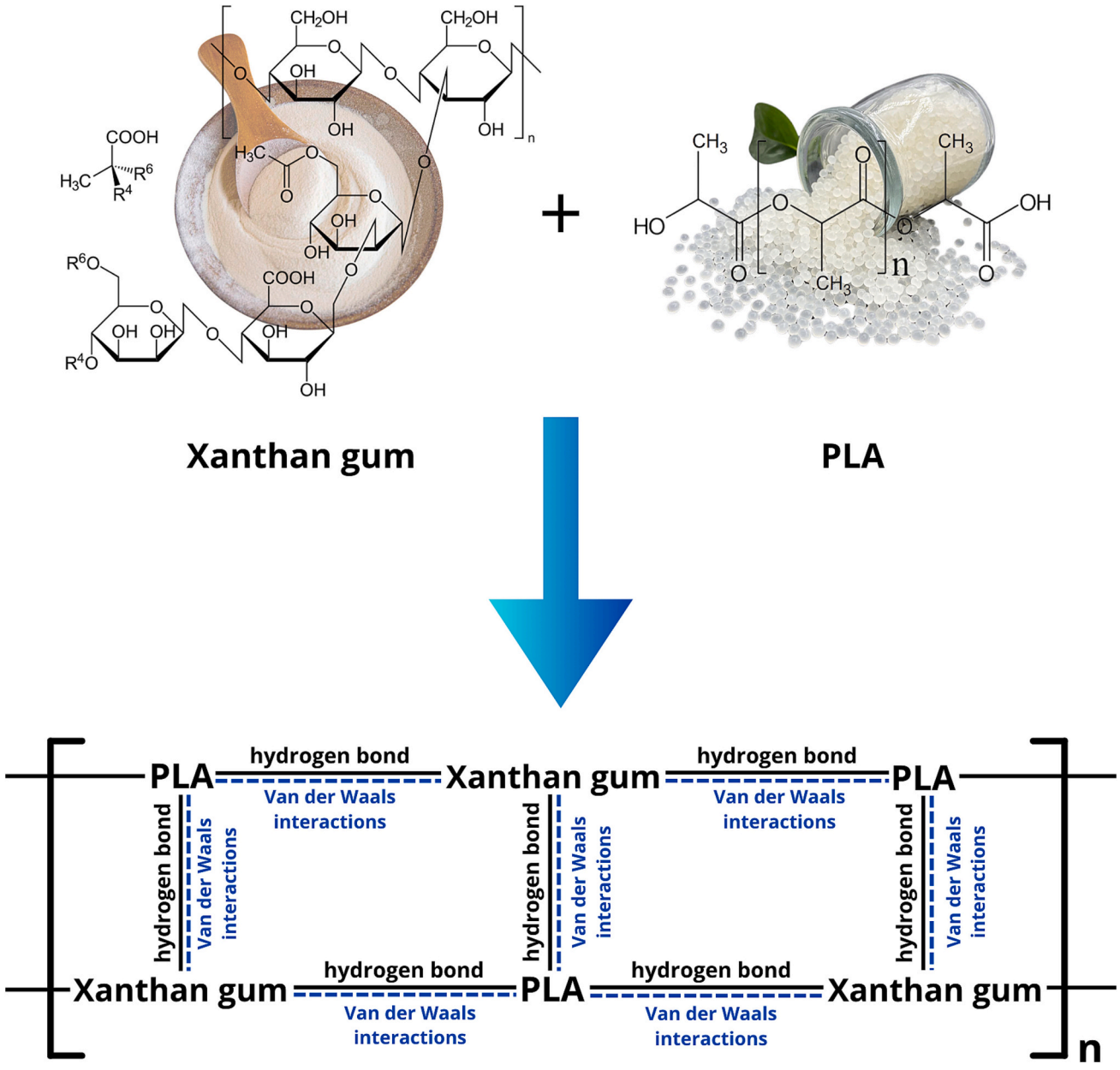

Fig. 1. Synthesis of XA/PLA aerogels and possible final structure.

2.2.17. Statistical analysis

All the experimental data are reported as mean ± standard deviation (SD). The statistical analysis was performed using SPSS Statistics 29 software (IBM, Armonk, NY, USA). The Shapiro-Wilk test was conducted to assess the normality of the data. Due to non-normal distribution, a Kruskal-Wallis test was applied to determine the differences between the groups. A p-value of <0.05 was considered statistically significant.

3. Results and discussion

3.1. Synthesis of XA/PLA-CSD aerogels

In this work, XA and PLA were used to develop hybrid aerogels by a sol-gel process and supercritical drying with CO_2. In the first step of the synthesis, the XA was dissolved in water, and the PLA was dissolved in ethyl lactate, resulting in two separate homogeneous solutions. After these starting solutions were mixed, the gelation process was initiated by an antisolvent mechanism. In this context, water acts as a nonsolvent for the PLA, causing it to precipitate and interact with the XA molecules. Gelation occurred by physical cross-linking between the XA and PLA, particularly through the formation of hydrogen bonds and Van der Waals interactions between the hydroxyl groups of XA and the carboxyl and ester groups of the PLA, as shown in Fig. 1. In the next step, absolute ethanol was added to the gel to remove the primary solvents (water and ethyl lactate) from the pores, as this step is crucial for producing aerogels. By removing the solvents, ethanol facilitated the formation of a more efficient network between the polysaccharide and the biopolymer and promoted hydrogen bonding. As we have reported previously [55], ethanol also reduced the repulsion between the hydrophilic chains of XA, allowing them to approach each other and interact more effectively with the PLA, which led to an improvement in the integrity and stability of the gel network. The resulting gel had a heterogeneous structure, in which the XA formed a hydrophilic backbone, while the PLA contributed hydrophobic segments that created a stable, interconnected network. This phenomenon benefits from the mechanical strength of PLA and the flexibility and water retention abilities of the XA. The final step of the synthesis was supercritical drying, which resulted in the formation of an aerogel with the same structure as the initial alcogel, but with gaseous CO_2 in its pores instead of alcohol. When SC CO_2 is used in the synthesis of aerogels, the porosity and high specific surface area are preserved, which are important properties for applications in wound healing. The appearance of the finished cotton-like aerogels can be seen in Figs. 3. a and b.

3.2. N_2 adsorption-desorption analysis

The compositions of the aerogels, along with their specific surface area and average pore sizes, are summarised in Table 1. These properties are crucial for wound healing applications, as they influence fluid absorption, gas exchange, and the release of the therapeutic agents. The results indicate that the XA/PLA2 aerogel had a slightly higher specific surface area (396 ± 8 m^2/g) than the XA/PLA1 (342 ± 7 m^2/g), which can be attributed to its greater XA content. XA is known for its ability to form highly porous networks; an increased proportion of XA likely contributed to the formation of a more open structure with enhanced surface area. Both reference aerogels exhibited similar average mesopore sizes, with XA/PLA2 having a slightly smaller value, aligning with its larger surface area. The specific surface area of XA/PLA-CSD aerogels was also measured for comparison. As shown in Table 1, these aerogels had a much lower surface area than XA/PLA1 and XA/PLA2. We hypothesise that this decrease was caused by the infiltration of active ingredients into the porous network, blocking the pores and limiting

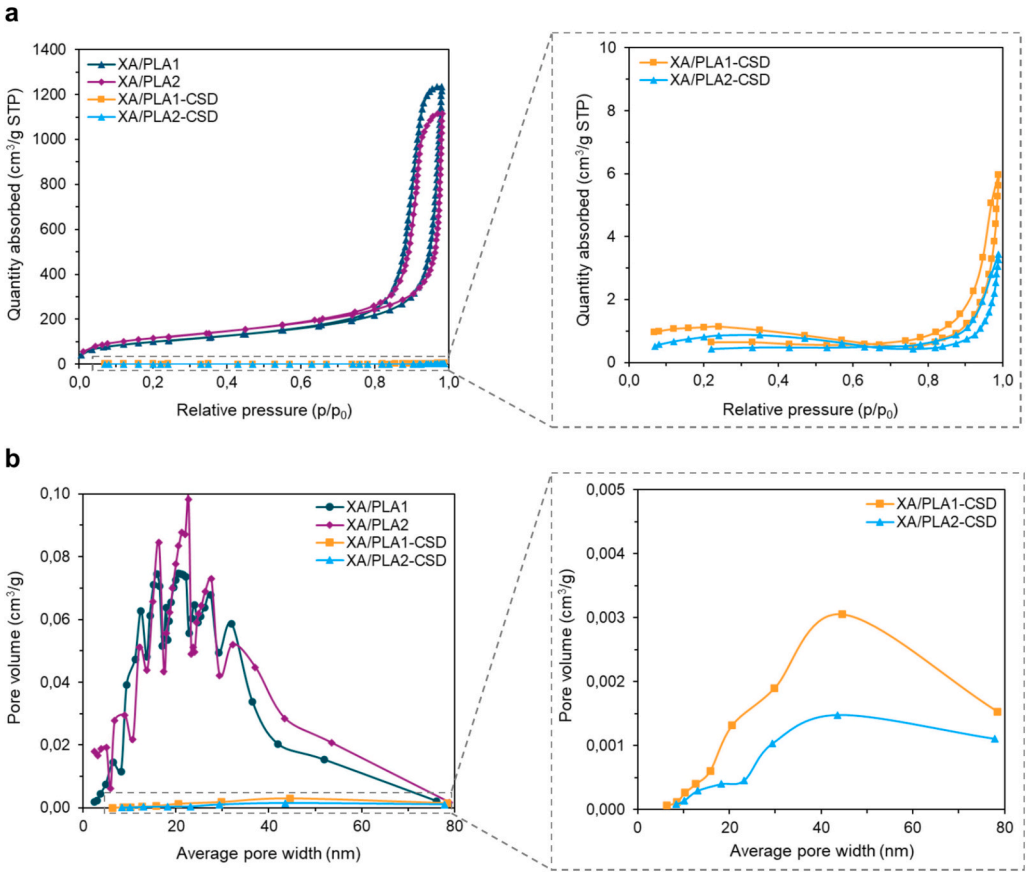

Fig. 2. a) N_2 physisorption isotherms of the XA/PLA and XA/PLA-CSD aerogels. b) BJH pore size distribution of the XA/PLA and XA/PLA-CSD aerogels.

their accessibility. The presence of DEX, along with the oxygen-generating agents CPO and SPO, likely have contributed to the formation of a denser structure, and thus reduced the overall porosity. The adsorption isotherms of the aerogels, shown in Fig. 2. a, further confirm these structural differences. All the tested aerogels exhibited typical IUPAC IV adsorption-desorption hysteresis with either H1 or H4 loops [56]. H1-type loops are characteristic of porous materials with well-aligned cylindrical pores and relatively narrow pore size distributions. In contrast, H4 loops are associated with complex materials containing both micro- and mesopores. This indicates that XA/PLA aerogels had typical mesoporous structures [56], which is also evident from the average pore width distribution (Fig. 2. b). The presence of mesopores is particularly beneficial for wound healing applications, as mesoporous materials have been shown to facilitate the adsorption and sustained release of bioactive compounds, thereby improving therapeutic efficiency [57]. The high adsorption capacities observed for the aerogels XA/PLA1 and XA/PLA2 suggest that these aerogels are excellent carriers for active ingredients. Despite their compositional differences, both aerogels exhibited similar adsorption potentials and mesopore volumes. On the other hand, the XA/PLA-CSD aerogels showed negligible N_2 adsorption capacity, indicating the near-complete absence of available pores, as the pores of the materials were filled with DEX and oxygen-generating agents.

3.3. SEM analysis

The morphology and microstructure of the aerogels were analysed with SEM (Fig. 3.). Both materials exhibited a fibrous network, with XA/PLA1-CSD having a slightly denser structure, which aligns with its lower specific surface area measured by N_2 adsorption-desorption analysis. The formation of these fibrous structures can be attributed to the addition of PLA, as reported previously [9]. Additionally, SEM images in Figs. 3. a and b confirm the porous nature of both aerogels. To assess the integration of active ingredients within the internal structure of the XA/PLA-CSD aerogels, SEM was also employed. By using higher magnifications, the presence of crystalline structures was observed, confirming the successful incorporation of oxygen-generating agents (CPO and SPO). Specifically, the cubic crystals characteristic of SPO [58] and rod-shaped CPO crystals, which tend to aggregate into a flower shape [59], were identified (Fig. 5. a). These findings indicate that the active ingredients were well distributed within the aerogel matrix, suggesting strong physical interactions between the aerogel framework and the incorporated compounds.

3.4. Thermal analysis

The decomposition of the XA/PLA1, XA/PLA2, XA/PLA1-CSD, and XA/PLA2-CSD aerogels was studied with thermal analysis, which included simultaneous TGA (Fig. 4. a) and DSC (Fig. 4. b) analyses.

The TGA thermograms (Fig. 4. a) revealed similar thermal degradation behaviour of the materials. The decomposition of the reference aerogels (XA/PLA1 and XA/PLA2) followed a two-step degradation process. The first mass loss occurred around 100 °C and is associated with the evaporation of moisture and volatile substances. This initial decrease was followed by a major decomposition in the temperature range of 220–400 °C due to the combined degradation of the XA and

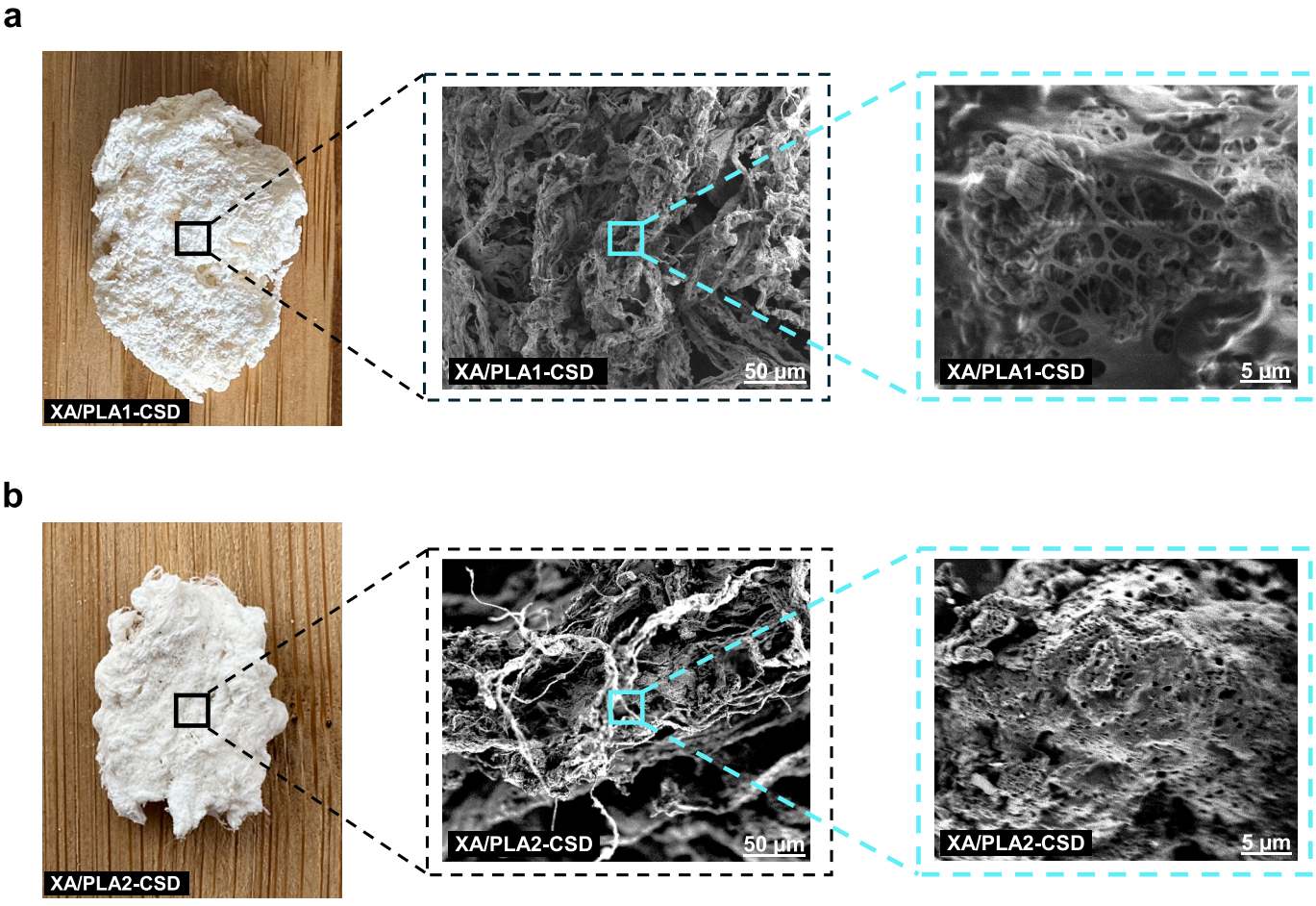

Fig. 3. a) The appearance of the XA/PLA1-CSD aerogel and SEM pictures at lower magnification and higher magnification. b) The appearance of the XA/PLA2-CSD aerogel and SEM pictures at lower and higher magnifications.

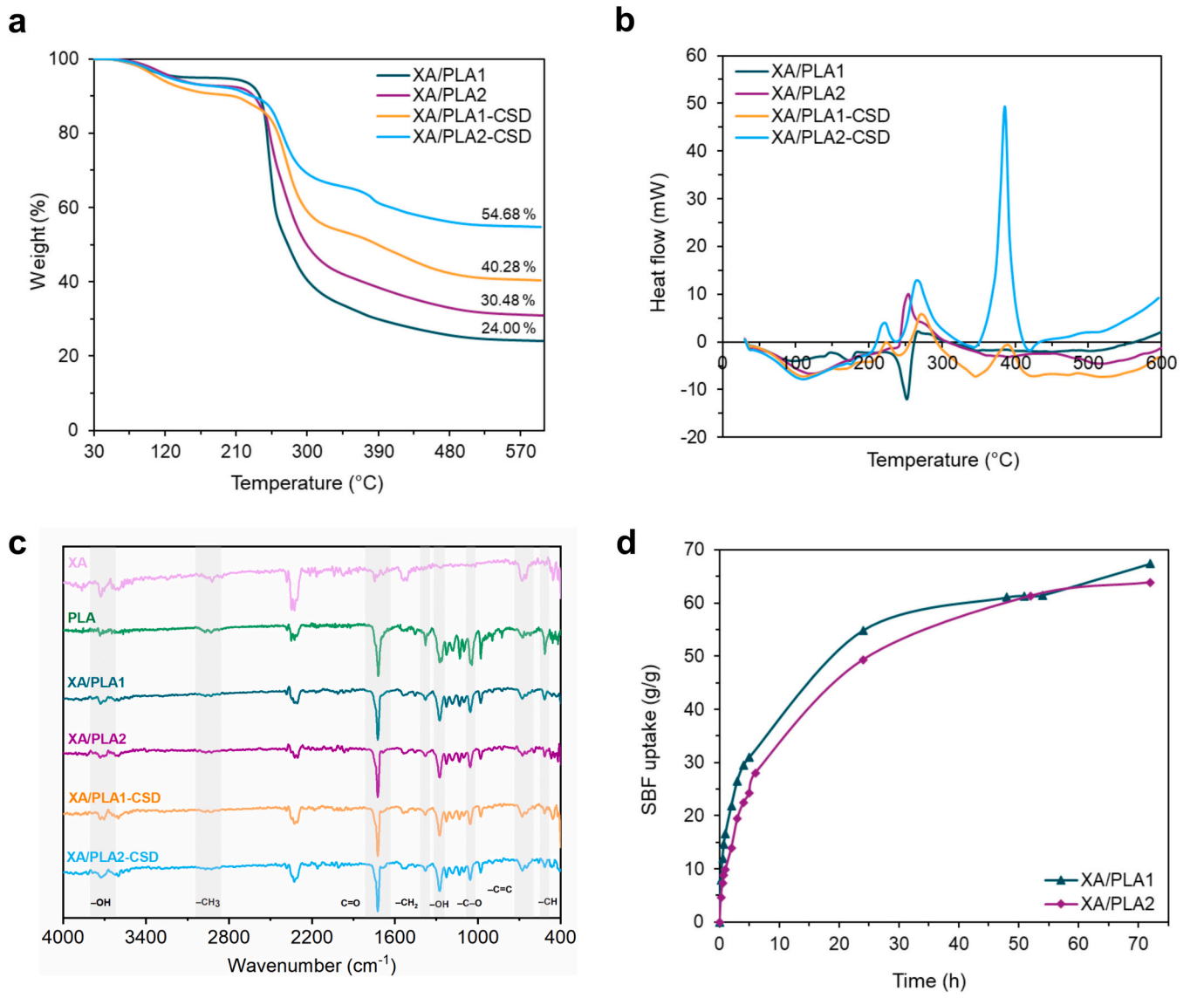

Fig. 4. a) TGA curves of the aerogels. b) DSC curves of the aerogels. c) FTIR spectra of the aerogels. d) Swelling of the reference XA/PLA aerogels.

PLA, resulting in approximately 70% weight loss. In contrast, the XA/PLA-CSD aerogels exhibited a three-step degradation process. Similar to the reference aerogels, the initial mass loss at 100 °C corresponded to water evaporation. The second degradation step at around 220 °C corresponded to the degradation of the XA and PLA. However, the addition of active ingredients introduced a third degradation step between 320 and 480 °C, where the decomposition proceeded more gradually. Among all samples, XA/PLA2-CSD showed the highest thermal stability and retained 55% of its original weight. DSC analysis (Fig. 4. b) further confirmed the thermal transitions observed in TGA. The reference aerogels (XA/PLA1 and XA/PLA2) exhibited an initial endothermic peak at 100 °C, corresponding to moisture loss, which aligns with the first degradation step in the TGA thermograms. Exothermic peaks at approximately 250 °C and 380 °C were also detected, marking the thermal decomposition of the aerogel components. For XA/PLA1-CSD and XA/PLA2-CSD, a similar trend was observed, with endothermic and exothermic transitions occurring at comparable temperatures. However, the exothermic events were more pronounced, indicating a higher energy release associated with the degradation of the active ingredients. This suggests that the incorporated compounds influence the thermal decomposition pathway, likely by altering the structural integrity of the aerogel framework. Overall, the TGA and DSC results confirm that the addition of active ingredients modifies the thermal stability of the aerogels. The introduction of oxygen-generating agents appears to delay complete degradation.

3.5. ATR-FTIR

The molecular structures of the XA/PLA-CSD and the XA/PLA aerogels were characterised by ATR-FTIR (Fig. 4. c). The aerogels are synthesised from a combination of XA and PLA, both of which have a high number of hydroxyl (O—H) and carboxyl (C=O) groups in their structure [60,61]. In the spectra shown in Fig. 4. c, the stretching between 3500 and 3800 cm^{-1} corresponds to O—H groups and intramolecular hydrogen bonds. Similar stretching is characteristic of XA, as reported previously by Pawlicka et al. [60] when the properties of this polysaccharide were studied. Additionally, -CH_3 stretching at 2800–3000 cm^{-1}, which also belongs to XA, is evident. The presence of PLA in the aerogels can be confirmed by a sharp peak at 1722 cm^{-}1, representing the C═O vibration of the ester bonds, characteristic of the PLA polymer, observed in all the materials [9,61]. Furthermore, the region of 1500–1400 cm^{-1} represents the stretching characteristic of the -CH_2 groups of XA. The spectra at 1275 cm^{-1} show a peak belonging to the C—O vibration within the carbonyl functional group of the PLA [61].

Moreover, the peaks at 1078 cm^{-1} and 978 cm^{-1} represent the C—O group, followed by the fingerprint region, where stretching between 600 and 500 cm^{-1} is attributed to the -CH vibrations of XA [60]. A comparison of the spectra of the reference (XA/PLA1, XA/PLA2) aerogels and XA/PLA-CSD aerogels revealed that all the peaks matched. The characteristic peaks of the active ingredients incorporated in our material (CPO, SPO, and DEX) either coincided with the peaks of the reference aerogels or were not visible in the spectra. Their absence could be due to their low concentration.

3.6. ToF-SIMS analysis

The ToF-SIMS measurements were performed to determine the DEX distribution in the XA/PLA2-CSD aerogel. Fig. 5. b presents a three-dimensional ToF-SIMS image of an aerogel sputtered with a 2.5 keV Ar^{+}_{1900} sputter beam for 4000 s to perform depth profiling. This sputtering was performed with GCIB, to preserve the chemical integrity of the aerogel during the acquisition of three-dimensional images. The ToF-SIMS image in Fig. 5. b illustrates the spatial distribution of F^{-} at *m/z* 19.00 (green spots), representing DEX [40,62]. The DEX is located within the porous structure of the aerogel, resulting in regions of higher intensity. Such localisation is typical in aerogels, which are known for their ability to incorporate active ingredients within their porous framework. Moreover, Fig. 5. b also shows the distribution of the CH^{-} signal at *m/z* 13.01 (red spots), which is attributed primarily to the structural composition of the aerogel matrix itself. Distribution analysis

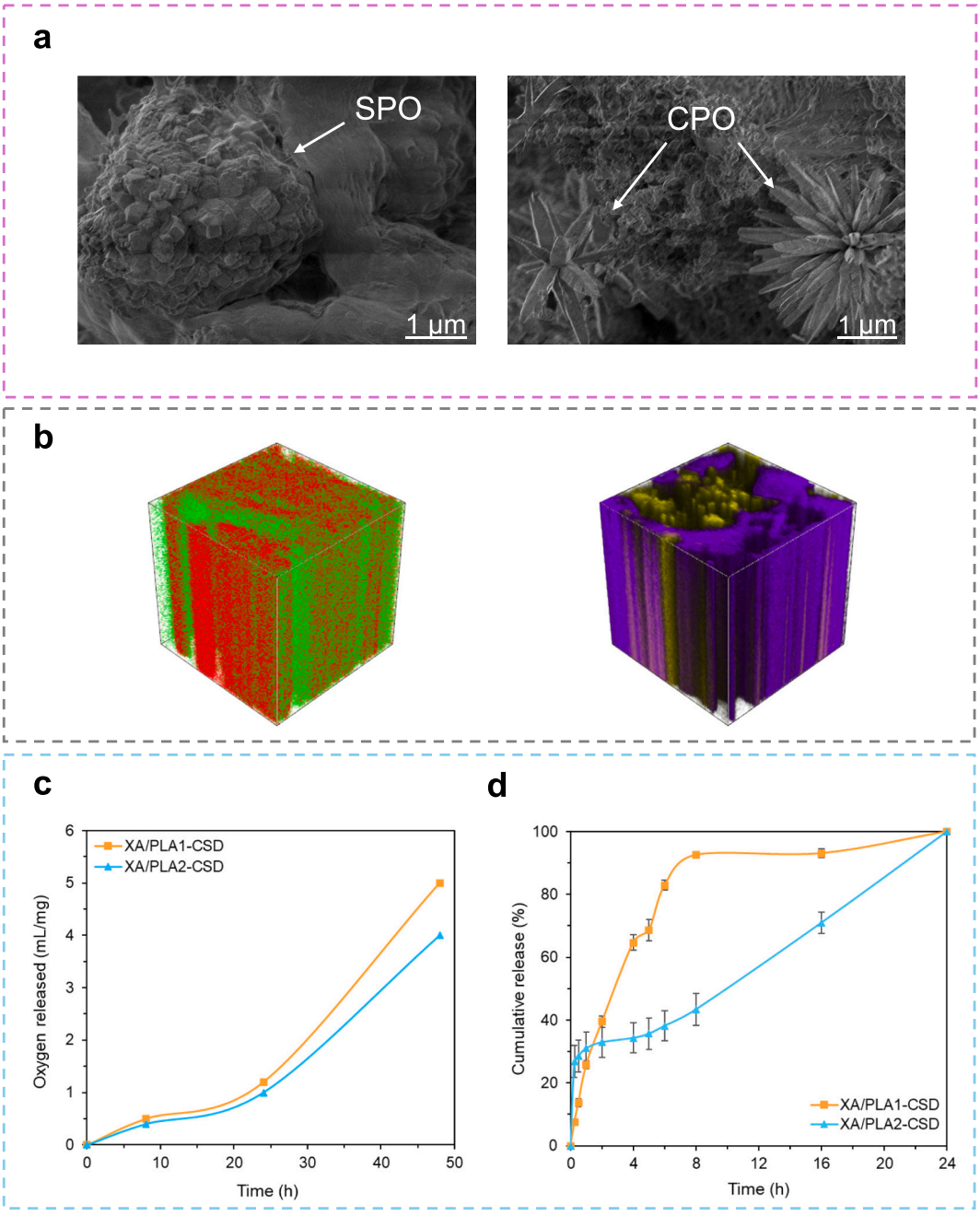

Fig. 5. **a)** SEM pictures showing crystals of SPO and CPO. **b)** 3D ToF-SIMS imaging of the XA/PLA2-CSD aerogel in negative polarity (red represents the CH^{-} signal, and green represents the F^{-} signal) and in positive polarity (purple represents the signal for Na^{+} and yellow represents the signal for Ca^{+}). The ToF-SIMS analysis was performed on an area of 300 × 300 μm, while the sputtered area was 500 × 500 μm. **c)** Oxygen release from XA/PLA-CSD aerogels. **d)** DEX release profiles in SBF at pH 7.2.

of the oxygen-generating components (CPO with the molecular formula CaO_2 and SPO with $Na_2H_3CO_6$) within the XA/PLA2-CSD aerogel was performed with positive ToF-SIMS polarity. The signals for Ca^+ at *m/z* 39.96 and Na^+ at *m/z* 22.99 in Fig. 5. b represent the distributions of CaO_2 and $Na_2H_3CO_6$, with purple representing the signals for Na^+ and green for Ca^+, respectively. The distribution of these signals across the analysed region indicates that the oxygen-generating components are not distributed homogeneously in the aerogel at the micron scale. Aerogels typically exhibit a wide distribution of pore sizes, ranging from micropores (<2 nm) to mesopores (2–50 nm) and macropores (>50 nm) [56]. This heterogeneity can lead to an uneven distribution of the active ingredients. Furthermore, the active ingredient loading method plays a crucial role in determining the substance's final distribution within the aerogel. Due to the constraints of its 3D network structure, the diffusion of drug molecules may be limited, leading to an uneven distribution [19]. This distribution indicates that, although the active component is not distributed uniformly in the aerogel, it is present in the material and is released effectively. Despite this distribution, controlled drug release was achieved in both XA/PLA-CSD aerogels. This is because drug release from biodegradable aerogels depends more on the degradation rate of the matrix material than on the distribution of the molecules of the active components themselves [19].

3.7. Swelling and stability

The swelling properties of aerogels are critical for potential applications in wound healing. Polysaccharides represent an optimal choice in this regard, as they are hydrophilic and, therefore, capable of absorbing considerable quantities of exudate from the wound [14,18]. Furthermore, they can maintain an appropriate moisture level within the wound and release incorporated drugs as they swell [10]. However, aerogels synthesised from natural biopolymer-based materials tend to degrade in a humid environment. It is, therefore, essential to understand their swelling and degradation rates, as these parameters help to determine the time window for the material's actual use. To investigate these parameters, the aerogels were immersed in SBF, and the results are shown in Fig. 4. d. During the first hours, both aerogels exhibited a rapid mass increase due to the absorption of the SBF medium. As illustrated in Fig. 4. d, the mass of both aerogels increased throughout the experiment, reaching a maximum after 72 h, when the materials absorbed 67 and 64 times their weight, respectively. Consequently, both aerogels demonstrated a high swelling capacity due to the hydrophilic nature of the XA, which enhanced the liquid absorption capacity of the hybrid aerogels. Furthermore, it was observed that the aerogels remained stable and did not degrade during the measurements, indicating their suitability for use in moist environments, such as wounds.

3.8. Oxygen release

The ability of XA/PLA-CSD aerogels to release oxygen was evaluated over 48 h using the water displacement method. The mechanism behind oxygen release is based on the decomposition of the SPO and CPO embedded within the aerogel structure. These compounds are known for their ability to generate oxygen in a controlled and sustained manner when exposed to moisture [37,63]. Upon contact with a moist environment, CPO and SPO undergo stepwise reactions (8), (9), and (10) below [63].

For the CPO, the decomposition begins with the formation of calcium hydroxide ($Ca(OH)_2$) and H_2O_2:

$$CaO_{2(s)} + 2H_2O \rightarrow Ca(OH)_{2(s)} + H_2O_2 \quad (9)$$

For SPO, the decomposition involves the release of sodium ions, carbonate ions and H_2O_2:

$$(Na_2CO_3)\cdot 3H_2O_2 + H_2O \rightarrow 4Na^+ + 2CO_3^{2-} + 3H_2O_2 \quad (10)$$

Subsequently, H_2O_2 decomposes into oxygen and water:

$$2H_2O_2 \rightarrow O_2 + 2H_2O \quad (11)$$

These reactions enable a sustained release of oxygen, where the rate of release is influenced by the aerogel's composition, structure and interaction with water.

While this process generates oxygen, both CPO and SPO produce H_2O_2, which can be toxic to surrounding tissues if released in excess [30]. To address this, the enzyme catalase was added into the aerogels, catalysing the degradation of H_2O_2 and thereby mitigating toxicity and promoting faster oxygen production [63,64]. As shown in Fig. 5. c, the release of oxygen from both XA/PLA-CSD aerogels was slow and continuous during the first hours of the experiment. After 20 h, the rate of oxygen production increased and followed a linear trend until the end of the measurements. The total amount of oxygen released from the aerogels reached values of 4 and 5 mL/mg, respectively. The differences in oxygen release can be attributed to the variations in the aerogel's composition and the distribution of CPO and SPO within the structure. Despite these differences, the release of oxygen from both aerogels was controlled and sustained. The highly porous structure of the aerogels, combined with their high swelling abilities, allowed efficient SBF uptake and the gradual decomposition of CPO and SPO. The distribution of catalase within the aerogel matrix ensured consistent decomposition of H_2O_2 and thus contributed to a controlled release of oxygen [65]. The controlled release of oxygen from the XA/PLA-CSD aerogels makes them particularly suitable for treating highly hypoxic wounds, where oxygen supply is critical in all stages of healing. Sufficient oxygen promotes all the essential processes, such as collagen synthesis, cell proliferation and angiogenesis, which are often impaired under hypoxic conditions [30,37,65].

3.9. Drug loading and release

The loading capacity of both XA/PLA-CSD aerogels was low, with the XA/PLA1-CSD aerogel achieving a loading of 2.32 ± 0.75% and the XA/PLA2-CSD aerogel having an even lower capacity of 0.58 ± 0.005%. We hypothesise that this was due to the impregnation process. Drug loading was performed with a solvent exchange step. For this purpose, DEX was dissolved in ethanol, and the wet gels were immersed in the solution, allowing the drug to diffuse into the gel matrix. The penetration of DEX into the gel structure was limited by factors such as solvent compatibility, pore accessibility, and diffusion kinetics, which, ultimately, resulted in low drug loading. Afterwards, the wet gels were dried supercritically, where the ethanol was replaced with CO_2. During this process, some amount of the drug was washed out.

The release performance of the XA/PLA-CSD aerogels was evaluated using DEX as a model drug, and the release study was conducted over 24 h in SBF. Different release profiles were observed, as shown in Fig. 5. d. Specifically, the XA/PLA2-CSD aerogel, containing a higher concentration of XA, exhibited an initially faster release of DEX that slowed down after approximately 4 h and followed a linear release trend. In contrast, the XA/PLA1-CSD aerogel, which contained a lower amount of XA, showed a slower and more controlled release throughout the 24 h period. The distinct release behaviours observed between the two aerogels can be attributed to the structural and compositional differences between the formulations. In particular, the concentration of XA had a great influence on the swelling capacity of the aerogel. XA is highly hydrophilic, meaning it has a strong ability to absorb water and swell when exposed to aqueous environments like SBF [66]. The higher concentration in the XA/PLA2-CSD enhanced the SBF uptake and swelling, resulting in a faster release. In contrast, the XA/PLA1-CSD aerogel with a lower amount of XA showed slightly reduced swelling capacity, which led to a more controlled and gradual release of DEX over time. These results demonstrate that the release profiles of DEX from XA/PLA-CSD aerogels can be modulated by adjusting the concentration of XA. This ability to tailor the release profile is a valuable tool in the design of drug

delivery systems, allowing for either rapid or sustained drug release depending on the therapeutic needs.

3.10. Drug release kinetics

Understanding drug release kinetics and the mechanism of release is essential for all drug delivery systems, particularly in wound healing applications, where controlled and sustained drug release is crucial for effective treatment [4]. The drug release data of DEX from the XA/PLA-CSD aerogels were fitted to commonly used kinetic models. It should be noted that the Korsmeyer-Peppas model was applied only to the initial 60% of drug release and was, therefore, suitable for analysing the early-stage release kinetics in this study [67]. The correlation coefficient (R^2) values for each model and the corresponding mechanism of release are presented in Table 2. The plots for the theoretical prediction of drug release kinetics are provided in the Supplementary material (Section S4).

The drug release kinetics of the XA/PLA-CSD aerogels demonstrated a clear correlation between the aerogel composition and the release mechanism. For the XA/PLA1-CSD aerogel, which had a higher XA content, the Korsmeyer-Peppas model provided the best fit to the release profile ($R^2 = 0.9825$). With an *n* value of 0.6606, it indicated a non-Fickian release mechanism (anomalous transport), meaning that both drug diffusion and polymer relaxation contributed to the release process. The higher XA content promoted swelling and matrix relaxation, which altered the diffusion pathway and resulted in a more complex release behaviour. In contrast, the XA/PLA2-CSD aerogel, with a higher proportion of PLA, showed the best fit with the zero-order model ($R^2 = 0.979$), indicating a constant drug release rate over time. The Korsmeyer-Peppas model also provided a good fit ($R^2 = 0.9084$), with an *n* value of 0.1119, which correlates to Fickian diffusion, where the diffusion controls primarily the drug release through the polymer matrix. The PLA, being a hydrophobic material, likely restricted swelling and matrix relaxation, leading to a more straightforward diffusion-controlled release profile. These findings highlight the influence of aerogel composition on drug release mechanisms, demonstrating that the release profile can be tailored to meet specific application requirements.

3.11. Biocompatibility and safety of aerogels

3.11.1. Antibacterial activity

Bacterial infections are a common issue in chronic wounds, as these provide a favourable environment for bacterial colonisation. Infections occur when bacteria, such as *E. coli* and *S. aureus*, colonise the wound and form biofilms that can delay the healing process, cause pain and potentially lead to severe complications [53]. To prevent such complications, it is advantageous for the material to possess antibacterial properties, as this is beneficial to the wound-healing process. The antibacterial activity of XA/PLA-CSD aerogels was evaluated with the agar diffusion method, and the results are shown in Fig. 6. a. Both XA/PLA-CSD aerogels demonstrated strong antibacterial activity against *E. coli* (ATCC 25922) and *S. aureus* (ATCC 29213) strains, as evidenced by the zones of inhibition (ZOI) around the samples on the agar plates. The diameters of ZOI against *E. coli* were 14 and 15 mm, while against *S. aureus*, the ZOI diameters were 30 and 31 mm, respectively. The results are summarised in Table 3 and illustrated in Fig. 6. b. Notably, the XA/PLA-CSD aerogels exhibited a stronger inhibitory effect against *S. aureus* (Gram-positive) than against *E. coli* (Gram-negative), likely due to the structural differences in the cell walls of the Gram-positive and Gram-negative bacteria. We hypothesise that the antibacterial properties of the XA/PLA-CSD aerogels result from the incorporation of active substances (CPO, SPO, and DEX), which is supported by the findings from the *in vitro* drug release studies. In these studies, the DEX was released within 24 h, reducing bacterial load, while the oxygen was released over 48 h, inhibiting further bacterial growth. The production of ROS during the decomposition of the CPO and SPO into oxygen enhanced the antibacterial effect, as ROS are known to disrupt bacterial cell membranes and other vital cellular components. They induce lipid peroxidation, disrupt membrane integrity and increase permeability, which leads to leakage of intracellular contents and loss of membrane potential. While bacteria can activate stress responses to counteract oxidative damage, excessive ROS levels overwhelm these defences, resulting ultimately in bacterial death. [68]. Therefore, both the XA/PLA1-CSD and XA/PLA2-CSD aerogels demonstrated strong antibacterial activity and showed promise in preventing bacterial colonisation.

The control plates (termed CONTROL in Fig. 6. a) were used to detect possible contamination. The absence of irregular microbial growth indicated that the agar plates used for the tests were free from contamination, and that the bacterial strains exhibited typical growth patterns.

3.11.2. Cell viability

Before any *in vivo* testing, it is essential to assess the cytocompatibility of newly developed materials. In this context, cell viability assays are crucial for evaluating a material's cytotoxicity and biocompatibility, ensuring that it supports cell growth and proliferation, which are vital for tissue regeneration [69,70]. The confirmation of high cell viability allows the prediction of the efficiency of the material in promoting wound healing, and the validation of its safety for use in biomedical applications [69]. For this purpose, cell viability tests were performed, and the results were obtained after 24 and 72 h. The experimental process is shown in Fig. 7. c. The results presented in Fig. 7. a demonstrate that the reference aerogels containing only XA and PLA (XA/PLA1, XA/PLA2) exhibited excellent cell viability of almost 100% after 24 and 72 h, indicating their cytocompatibility. Similar cytocompatibility was observed when DEX, SPO, and catalase were incorporated into the aerogels (XA/PLA2-SD), confirming the safety of integrating these agents at the tested concentrations. However, the formulation containing both CPO and SPO reduced the viability of NIH/3T3 cells significantly. This reduction can be attributed to excessive ROS production during the decomposition of both oxygen-generating agents. Despite the presence of catalase, the amount of H_2O_2 produced was overwhelming to the defence mechanisms of the cells and resulted in oxidative stress and cellular damage. In contrast, SPO alone generated oxygen more efficiently with less H_2O_2 production, which resulted in higher cell viability. Adjusting the concentrations of CPO and catalase could help to reduce the observed cytotoxicity in these formulations.

3.11.3. Hemolytic activity

Hemolysis refers to the rupture or destruction of red blood cells, releasing hemoglobin into the surrounding plasma [70]. This process can lead to a variety of complications, such as inflammation, anemia, and other systemic issues [71]. When a material is applied to the wound,

Table 2
R^2 values, *n* and mechanism of drug release determined for the XA/PLA-CSD aerogels.

Sample	Zero−order	First−order	Higuchi model	Korsmeyer−Peppas		Mechanism of release
	R^2	R^2	R^2	R^2	*n*	
XA/PLA1−CSD	0.639	0.8893	0.8773	0.9825	0.6606	Non-Fickian
XA/PLA2−CSD	0.979	0.8267	0.8807	0.9084	0.1119	Fickian

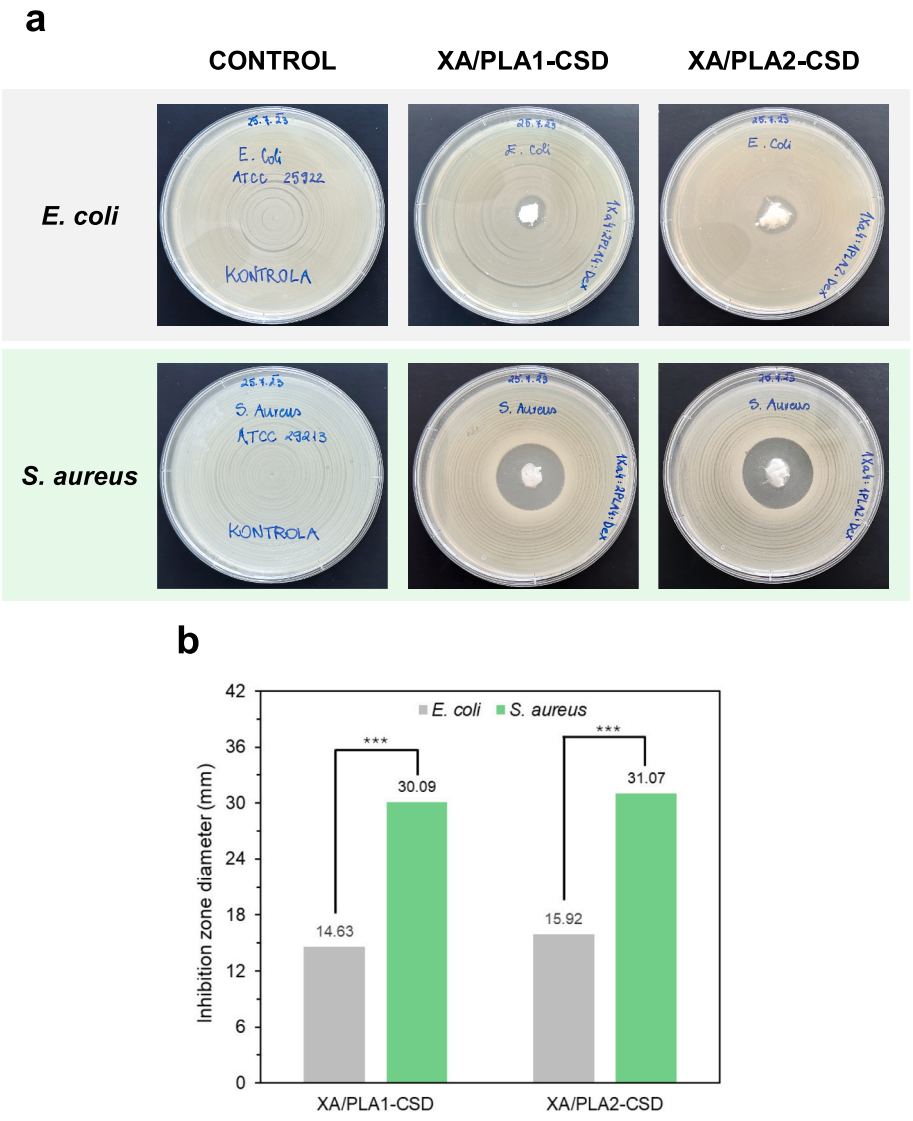

Fig. 6. a) Antibacterial activity of the XA/PLA-CSD aerogels against *E. coli* (ATCC 25922) and *S. aureus* (ATCC 29213) after 48 h of incubation. b) Inhibition zone diameters (mm) of the XA/PLA-CSD aerogels against *E. coli* (ATCC 25922) and *S. aureus* (ATCC 29213) after 48 h of incubation. The asterisks represent the significance value: $p < 0.001$ (***).

Table 3
Inhibition zone dimeters (d) against *E. coli* and *S. aureus* after 48 h of incubation.

Sample	d (mm)	
	48 h	
	E. coli	*S. aureus*
XA/PLA1-CSD	14.63 ± 0.3	30.09 ± 0.8
XA/PLA2-CSD	15.92 ± 0.4	31.07 ± 1.0

it first interacts with blood, making it essential to assess its hemocompatibility. Therefore, evaluating a material's potential to cause hemolysis is an important step in determining whether it is safe for *in vivo* applications [70]. A material is considered hemocompatible if it induces a lysis rate of no >5% when in direct contact with red blood cells. Any material that exceeds this level would be deemed unsafe for blood contact [72,73]. In this study, hemolysis assays were performed by directly exposing the aerogels to human blood. The resulting data, shown in Fig. 7. b, demonstrate that all the aerogels exhibited negligible hemolytic activity, with values ranging from −1% to 2%. These results indicate that none of the aerogels caused any significant rupture of red blood cells, making them promising candidates for biomedical applications involving blood contact. Similar results were observed for polycaprolactone (PCL) and for methylcellulose-based aerogel scaffolds [69,74]. The comparison with control groups further emphasises the significance of the results. The positive control, Triton X-100, a known surfactant that induces complete lysis of red blood cells, showed 100% hemolysis, while the negative control, PBS at pH 7.4, showed no hemolysis, as expected for a non-hemolytic solution. Overall, the negligible hemolytic activity of the aerogels suggests they could be used in applications such as wound healing, drug delivery systems or tissue engineering, where direct contact with human blood occurs. However, additional *in vitro* and *in vivo* tests are necessary to assess other important aspects of biocompatibility, including the material's interaction with platelets and plasma.

4. Conclusion

In this study, hybrid XA/PLA-CSD aerogels loaded with oxygen-generating agents CPO and SPO and the anti-inflammatory drug DEX

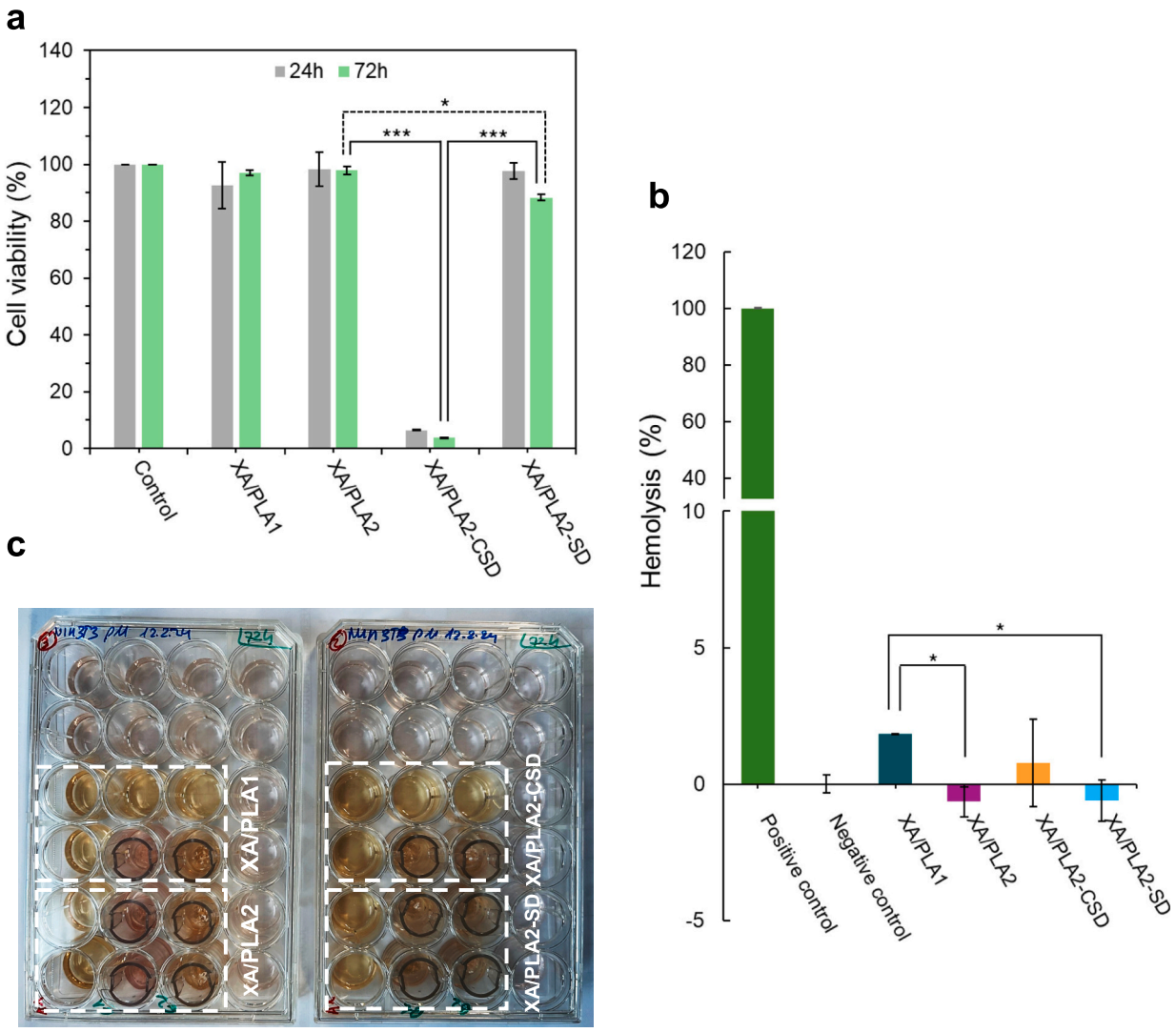

Fig. 7. a) Viability of NIH/3T3 cells after 24 and 72 h of contact with different aerogel formulations. b) The hemolytic activity of different aerogel formulations (positive control: 4% (v/v) Triton X-100 solution; negative control: PBS pH 7.4 solution). c) The process of the cell viability test. The asterisks represent the following significance values: $p < 0.05$ (*), $p < 0.001$ (***).

were developed successfully as potential wound dressing materials. The aerogels had a highly porous structure with a high specific surface area. The addition of PLA improved the stability of the aerogels in SBF and increased their swelling capacity, both of which are crucial for wound healing applications. The *in vitro* drug release tests demonstrated the controlled and sustained release, which could impact the wound healing process positively. The release profile of DEX from the XA/PLA1-CSD aerogel followed the Korsmeyer-Peppas kinetic model, indicating a non-Fickian release mechanism. In contrast, DEX release from the XA/PLA2-CSD aerogel was governed by Fickian diffusion, with the best fit observed with the zero-order model. Additionally, the aerogels inhibited the growth of *E. coli* and *S. aureus* effectively, demonstrating strong antibacterial activity. The cell viability assays with mouse fibroblasts (NIH/3T3) confirmed the biocompatibility of the XA/PLA-SD aerogels, while the addition of CPO led to reduced viability. Finally, the hemocompatibility analysis revealed excellent results, as no hemolytic activity was observed. These findings highlight the multifunctionality of the XA/PLA-CSD aerogels, addressing essential aspects of wound care through synergistic healing effects. Despite these encouraging results, several limitations need to be addressed in future research. First, *in vivo* studies are crucial to assess the material's biocompatibility, long-term stability, and effectiveness in promoting wound healing. Additionally, the current cytocompatibility assessment was limited to NIH/3T3 mouse fibroblasts; further testing on other relevant cell types, such as endothelial or epidermal cells, is required to gain a comprehensive understanding of the material's interactions with biological systems. The combination of CPO and SPO led to reduced cell viability due to excessive ROS production, even with the inclusion of catalase. Further studies should optimise the concentrations of CPO and catalase or use solely SPO as the oxygen-generating agent. While the aerogels demonstrated excellent swelling and biodegradability, their mechanical properties under physiological conditions, such as tensile strength in moist environments, were not evaluated. Variations in the composition of the XA/PLA aerogels, such as the ratio of XA to PLA or the concentration of oxygen-generating agents, significantly affected both the drug release profiles and cell viability. This suggests that a more detailed investigation is needed to better understand how these compositional factors influence the overall performance of the aerogels. Additionally, the rates of oxygen release and their impact on wound healing require more investigation. Finally, scaling up the production of these aerogels for clinical applications presents challenges in terms of reproducibility, cost and regulatory compliance.

CRediT authorship contribution statement

Nika Atelšek Hozjan: Writing – review & editing, Writing – original draft, Methodology, Investigation, Formal analysis, Data curation. **Gabrijela Horvat:** Writing – review & editing, Writing – original draft, Validation, Supervision, Methodology, Conceptualization. **Matjaž Finšgar:** Writing – review & editing, Writing – original draft, Formal analysis. **Ana Iglesias-Mejuto:** Writing – review & editing, Writing – original draft, Investigation, Formal analysis. **Inés Ardao Palacios:** Writing – review & editing, Methodology. **Carlos A. García-González:** Writing – review & editing. **Željko Knez:** Writing – review & editing, Resources, Project administration, Funding acquisition. **Zoran Novak:** Writing – review & editing, Project administration, Funding acquisition.

Declaration of competing interest

The authors declare that they have no known competing financial interests or personal relationships that could have influenced the work in this article.

Acknowledgements

The authors thank the Slovenian Agency for Research and Innovations (ARIS) for supporting the work of Research Programs P2-0046 and P2-0118. The Republic of Slovenia, the Ministry of Higher Education, Science and Innovation, and the European Union under the European Regional Development Fund are gratefully acknowledged for supporting the mentioned projects and for the use of an apparatus for supercritical drying, procured within the project "Upgrading national research infrastructures – RIUM". The authors also acknowledge the financial support from the COST CA18125 Advanced Engineering and Research of AeroGels for Environment and Life Sciences. The work was carried out in the framework of the COST Innovators Grant IG18125 "Technical, commercial and societal innovations on aerogels toward a circular economy" (ECO-AERoGELS) funded by the European Commission, and was also supported by MICIU/AEI 10.13039/501100011033 [Grants PID2020-120010RB-I00 and PDC2022-133526-I00], and by ERDF/EU and the European Union NextGeneration EU/PRTR. A.I.M. acknowledges Xunta de Galicia for her predoctoral research fellowship [ED481A-2020/104].

Appendix A. Supplementary data

Supplementary data to this article can be found online at https://doi.org/10.1016/j.ijbiomac.2025.143314.

Data availability

Additional results are presented in the Supplementary file. Other data will be made available on request.

References

[1] C.K. Sen, Human wound and its burden: Updated 2022 Compendium of Estimates, Adv. Wound Care 12 (2023) 657–670. doi:https://doi.org/10.1089/wound.2023.0150.
[2] Z. Yang, K. Ren, Y. Chen, X. Quanji, C. Cai, J. Yin, Oxygen-generating hydrogels as oxygenation therapy for accelerated chronic wound healing, Adv. Healthc. Mater. 13 (2024) 2302391, https://doi.org/10.1002/adhm.202302391.
[3] R. Zheng, L. Liu, H. Wang, P. He, F. Qi, S. Hu, X. Long, Z. Shi, G. Yang, Tai-chi hydrogel with Chinese philosophy and photothermal properties for accelerated diabetic wound healing, Adv. Compos. Hybrid Mater. 7 (2024) 43, https://doi.org/10.1007/s42114-024-00847-0.
[4] V. Falanga, R.R. Isseroff, A.M. Soulika, M. Romanelli, D. Margolis, S. Kapp, M. Granick, K. Harding, Chronic wounds, Nat. Rev. Dis. Primers. 8 (2022) 1–21, https://doi.org/10.1038/s41572-022-00377-3.
[5] X. Lin, X. Zhang, Y. Wang, W. Chen, Z. Zhu, S. Wang, Hydrogels and hydrogel-based drug delivery systems for promoting refractory wound healing: applications and prospects, Int. J. Biol. Macromol. 285 (2025) 138098, https://doi.org/10.1016/j.ijbiomac.2024.138098.
[6] H.P.S. Abdul Khalil, E. Bashir Yahya, F. Jummaat, A.S. Adnan, N.G. Olaiya, S. Rizal, C.K. Abdullah, D. Pasquini, S. Thomas, Biopolymers based aerogels: a review on revolutionary solutions for smart therapeutics delivery, Prog. Mater. Sci. 131 (2023) 101014, https://doi.org/10.1016/j.pmatsci.2022.101014.
[7] G. Yaşayan, O. Nejati, A.F. Ceylan, Ç. Karasu, P. Kelicen Ugur, A. Bal-Öztürk, A. Zarepour, A. Zarrabi, E. Mostafavi, Tackling chronic wound healing using nanomaterials: advancements, challenges, and future perspectives, Appl. Mater. Today 32 (2023) 101829, https://doi.org/10.1016/j.apmt.2023.101829.
[8] I. Savencu, S. Iurian, A. Porfire, C. Bogdan, I. Tomuță, Review of advances in polymeric wound dressing films, React. Funct. Polym. 168 (2021) 105059, https://doi.org/10.1016/j.reactfunctpolym.2021.105059.
[9] G. Horvat, K. Žvab, Ž. Knez, Z. Novak, Hybrid polylactic-acid-pectin aerogels: synthesis, structural properties, and drug release, Polymers 15 (2023) 407, https://doi.org/10.3390/polym15020407.
[10] S. Hasan, M.A. Hasan, M.U. Hassan, M. Amin, T. Javed, L. Fatima, Biopolymers in diabetic wound care management: a potential substitute to traditional dressings, Eur. Polym. J. 189 (2023) 111979, https://doi.org/10.1016/j.eurpolymj.2023.111979.
[11] W. Wang, S. Ummartyotin, R. Narain, Advances and challenges on hydrogels for wound dressing, Curr. Opin. Biomed. Eng. 26 (2023) 100443, https://doi.org/10.1016/j.cobme.2022.100443.
[12] X. Deng, M. Gould, M.A. Ali, A review of current advancements for wound healing: biomaterial applications and medical devices, J. Biomed. Mater. Res. B Appl. Biomater. 110 (2022) 2542–2573, https://doi.org/10.1002/jbm.b.35086.
[13] G. Horvat, M. Pantić, Ž. Knez, Z. Novak, Preparation and characterization of polysaccharide - silica hybrid aerogels, Sci. Rep. 9 (2019) 16492, https://doi.org/10.1038/s41598-019-52974-0.
[14] B.G. Bernardes, P. Del Gaudio, P. Alves, R. Costa, C.A. García-Gonzaléz, A. L. Oliveira, Bioaerogels: promising nanostructured materials in fluid management, healing and regeneration of wounds, Molecules 26 (2021) 3834, https://doi.org/10.3390/molecules26133834.
[15] G. Horvat, K. Xhanari, M. Finšgar, L. Gradišnik, U. Maver, Ž. Knez, Z. Novak, Novel ethanol-induced pectin–xanthan aerogel coatings for orthopedic applications, Carbohydr. Polym. 166 (2017) 365–376, https://doi.org/10.1016/j.carbpol.2017.03.008.
[16] S. Groult, S. Buwalda, T. Budtova, Tuning bio-aerogel properties for controlling drug delivery. Part 2: cellulose-pectin composite aerogels, Biomater. Adv. 135 (2022) 212732, https://doi.org/10.1016/j.bioadv.2022.212732.
[17] Y. Wang, J. Qi, M. Zhang, T. Xu, C. Zheng, Z. Yuan, C. Si, Cellulose-based aerogels, films, and fibers for advanced biomedical applications, Chem. Eng. J. 497 (2024) 154434, https://doi.org/10.1016/j.cej.2024.154434.
[18] H. Maleki, L. Durães, C.A. García-González, P. del Gaudio, A. Portugal, M. Mahmoudi, Synthesis and biomedical applications of aerogels: possibilities and challenges, Adv. Colloid Interface Sci. 236 (2016) 1–27, https://doi.org/10.1016/j.cis.2016.05.011.
[19] C.A. García-González, A. Sosnik, J. Kalmár, I. De Marco, C. Erkey, A. Concheiro, C. Alvarez-Lorenzo, Aerogels in drug delivery: from design to application, J. Control. Release 332 (2021) 40–63, https://doi.org/10.1016/j.jconrel.2021.02.012.
[20] N. Guo, Y. Xia, W. Zeng, J. Chen, Q. Wu, Y. Shi, G. Li, Z. Huang, G. Wang, Y. Liu, Alginate-based aerogels as wound dressings for efficient bacterial capture and enhanced antibacterial photodynamic therapy, Drug Deliv. 29 (n.d.) 1086–1099. doi:https://doi.org/10.1080/10717544.2022.2058650.
[21] Y. Chen, Y. Xiang, H. Zhang, T. Zhu, S. Chen, J. Li, J. Du, X. Yan, A multifunctional chitosan composite aerogel based on high density amidation for chronic wound healing, Carbohydr. Polym. 321 (2023) 121248, https://doi.org/10.1016/j.carbpol.2023.121248.
[22] D. Hua, S. Gao, M. Zhang, W. Ma, C. Huang, A novel xanthan gum-based conductive hydrogel with excellent mechanical, biocompatible, and self-healing performances, Carbohydr. Polym. 247 (2020) 116743, https://doi.org/10.1016/j.carbpol.2020.116743.
[23] B.Y. Bhardwaj, S. Vihal, R. Pahwa, S. Agarwal, B. Gupta, J.C. Yang, R. Chauhan, D. K. Chellappan, G. Gupta, S.K. Singh, K. Dua, P. Negi, Recent advancements in xanthan gum-based gastroretentive floating formulations: chemical modification, production and applications, Carbohydr. Polym. 348 (2025) 122809, https://doi.org/10.1016/j.carbpol.2024.122809.
[24] H.L. Chen, J.W.Y. Chung, V.C.M. Yan, T.K.S. Wong, Polylactic acid-based biomaterials in Wound healing: a systematic review, Adv. Skin Wound Care 36 (2023) 1, https://doi.org/10.1097/ASW.0000000000000011.
[25] P. Heydari, A. Zargar Kharazi, L. Shariati, Enhanced wound regeneration by PGS/PLA fiber dressing containing platelet-rich plasma: an in vitro study, Sci. Rep. 14 (2024) 12019, https://doi.org/10.1038/s41598-024-62855-w.
[26] H. Lee, D.Y. Shin, Y. Na, G. Han, J. Kim, N. Kim, S.-J. Bang, H.S. Kang, S. Oh, C.-B. Yoon, J. Park, H.-E. Kim, H.-D. Jung, M.-H. Kang, Antibacterial PLA/Mg composite with enhanced mechanical and biological performance for biodegradable orthopedic implants, Biomater. Adv. 152 (2023) 213523, https://doi.org/10.1016/j.bioadv.2023.213523.
[27] M. Wang, S.Y.H. Abdalkarim, R. Gong, H. Ji, Z. Chen, Y. Shen, Y. Zhou, J. Shen, H.-Y. Yu, Controlled long-term sustained release of poly(lactic acid) composite microspheres with dual-responsive cellulose nanocrystals, CrystEngComm 25 (2023) 4100–4110, https://doi.org/10.1039/D3CE00440F.
[28] S. Saghazadeh, C. Rinoldi, M. Schot, S.S. Kashaf, F. Sharifi, E. Jalilian, K. Nuutila, G. Giatsidis, P. Mostafalu, H. Derakhshandeh, K. Yue, W. Swieszkowski, A. Memic, A. Tamayol, A. Khademhosseini, Drug delivery systems and materials for wound healing applications, Adv. Drug Deliv. Rev. 127 (2018) 138–166, https://doi.org/10.1016/j.addr.2018.04.008.

[29] H. Li, B. Li, D. Lv, W. Li, Y. Lu, G. Luo, Biomaterials releasing drug responsively to promote wound healing via regulation of pathological microenvironment, Adv. Drug Deliv. Rev. 196 (2023) 114778, https://doi.org/10.1016/j.addr.2023.114778.
[30] N.G.A. Willemen, S. Hassan, M. Gurian, J. Li, I.E. Allijn, S.R. Shin, J. Leijten, Oxygen-releasing biomaterials: current challenges and future applications, Trends Biotechnol. 39 (2021) 1144–1159, https://doi.org/10.1016/j.tibtech.2021.01.007.
[31] D. Nolfi-Donegan, A. Braganza, S. Shiva, Mitochondrial electron transport chain: oxidative phosphorylation, oxidant production, and methods of measurement, Redox Biol. 37 (2020) 101674, https://doi.org/10.1016/j.redox.2020.101674.
[32] G.M. Gordillo, C.K. Sen, Revisiting the essential role of oxygen in wound healing, Am. J. Surg. 186 (2003) 259–263, https://doi.org/10.1016/S0002-9610(03)00211-3.
[33] R. Augustine, M. Gezek, N.S. Bostanci, A. Nguyen, G. Camci-Unal, Oxygen-generating scaffolds: one step closer to the clinical translation of tissue engineered products, Chem. Eng. J. 455 (2023) 140783, https://doi.org/10.1016/j.cej.2022.140783.
[34] A.A. Tandara, T.A. Mustoe, Oxygen in Wound healing?More than a nutrient, World J. Surg. 28 (2004) 294–300, https://doi.org/10.1007/s00268-003-7400-2.
[35] A. Al Mamun, A. Ullah, M.E.H. Chowdhury, H.E. Marei, A.P. Madappura, M. Hassan, M. Rizwan, V.G. Gomes, A. Amirfazli, A. Hasan, Oxygen releasing patches based on carbohydrate polymer and protein hydrogels for diabetic wound healing: a review, Int. J. Biol. Macromol. 250 (2023) 126174, https://doi.org/10.1016/j.ijbiomac.2023.126174.
[36] T. Agarwal, S. Kazemi, M. Costantini, F. Perfeito, C.R. Correia, V. Gaspar, L. Montazeri, C. De Maria, J.F. Mano, M. Vosough, P. Makvandi, T.K. Maiti, Oxygen releasing materials: towards addressing the hypoxia-related issues in tissue engineering, Mater. Sci. Eng. C 122 (2021) 111896, https://doi.org/10.1016/j.msec.2021.111896.
[37] Q. Bai, C. Zheng, N. Sun, W. Chen, Q. Gao, J. Liu, F. Hu, T. Zhou, Y. Zhang, T. Lu, Oxygen-releasing hydrogels promote burn healing under hypoxic conditions, Acta Biomater. 154 (2022) 231–243, https://doi.org/10.1016/j.actbio.2022.09.077.
[38] V.S. Madamsetty, R. Mohammadinejad, I. Uzieliene, N. Nabavi, A. Dehshahri, J. García-Couce, S. Tavakol, S. Moghassemi, A. Dadashzadeh, P. Makvandi, A. Pardakhty, A. Aghaei Afshar, A. Seyfoddin, Dexamethasone: insights into pharmacological aspects, therapeutic mechanisms, and delivery systems, ACS Biomater Sci. Eng. (2022), https://doi.org/10.1021/acsbiomaterials.2c00026 acsbiomaterials.2c00026.
[39] K. Qiu, B. Chen, W. Nie, X. Zhou, W. Feng, W. Wang, L. Chen, X. Mo, Y. Wei, C. He, Electrophoretic deposition of dexamethasone-loaded mesoporous silica nanoparticles onto poly(l-lactic acid)/poly(ε-Caprolactone) composite scaffold for bone tissue engineering, ACS Appl. Mater. Interfaces 8 (2016) 4137–4148, https://doi.org/10.1021/acsami.5b11879.
[40] M. Majrashi, A. Kotowska, D. Scurr, J.M. Hicks, A. Ghaemmaghami, J. Yang, Sustained release of dexamethasone from 3D-printed scaffolds modulates macrophage activation and enhances osteogenic differentiation, ACS Appl. Mater. Interfaces 15 (2023) 56623–56638, https://doi.org/10.1021/acsami.3c09774.
[41] J. Liu, L. Zhu, Y. Bao, Z. Du, L. Shi, X. Hong, Z. Zou, G. Peng, Injectable dexamethasone-loaded peptide hydrogel for therapy of radiation-induced ototoxicity by regulating the mTOR signaling pathway, J. Control. Release 365 (2024) 729–743, https://doi.org/10.1016/j.jconrel.2023.12.004.
[42] H. Tu, D. Zhang, A.N. Barksdale, M.C. Wadman, R.L. Muelleman, Y.-L. Li, Dexamethasone improves Wound healing by decreased inflammation and increased Vasculogenesis in mouse skin frostbite model, Wilderness Environ. Med. 31 (2020) 407–417, https://doi.org/10.1016/j.wem.2020.07.003.
[43] H.S. Channey, K. Holkar, V. Kale, G. Ingavle, Dexamethasone release pattern via a three-dimensional system for effective bone regeneration, Biomed. Mater. 18 (2023) 042003, https://doi.org/10.1088/1748-605X/acdb1e.
[44] M.-X. Ruiz-Caldas, C. Schiele, S.E. Hadi, M. Andersson, P. Mohammadpour, L. Bergström, A.P. Mathew, V. Apostolopoulou-Kalkavoura, Anisotropic foams derived from textile-based cellulose nanocrystals and xanthan gum, Carbohydr. Polym. 338 (2024) 122212, https://doi.org/10.1016/j.carbpol.2024.122212.
[45] R.B. Chim, M.B.C. De Matos, M.E.M. Braga, A.M.A. Dias, H.C. De Sousa, Solubility of dexamethasone in supercritical carbon dioxide, J. Chem. Eng. Data 57 (2012) 3756–3760, https://doi.org/10.1021/je301065f.
[46] T. Kokubo, H. Takadama, How useful is SBF in predicting in vivo bone bioactivity? Biomaterials 27 (2006) 2907–2915, https://doi.org/10.1016/j.biomaterials.2006.01.017.
[47] N. Hassanzadeh Nemati, E. Ghasempour, A. Zamanian, Effect of dual releasing of β-glycerophosphate and dexamethasone from Ti nanostructured surface for using in orthopedic applications, Int. J. Eng. 32 (2019) 1337–1344, https://doi.org/10.5829/ije.2019.32.10a.01.
[48] M.-L. Laracuente, M.H. Yu, K.J. McHugh, Zero-order drug delivery: state of the art and future prospects, J. Control. Release 327 (2020) 834–856, https://doi.org/10.1016/j.jconrel.2020.09.020.
[49] M. Rostamitabar, R. Subrahmanyam, P. Gurikov, G. Seide, S. Jockenhoevel, S. Ghazanfari, Cellulose aerogel micro fibers for drug delivery applications, Mater. Sci. Eng. C 127 (2021) 112196, https://doi.org/10.1016/j.msec.2021.112196.
[50] D.R. Paul, Elaborations on the Higuchi model for drug delivery, Int. J. Pharm. 418 (2011) 13–17, https://doi.org/10.1016/j.ijpharm.2010.10.037.
[51] T.J. Hossain, Methods for screening and evaluation of antimicrobial activity: a review of protocols, advantages, and limitations, Eur. J. Microbiol. Immunol. 14 (2024) 97–115, https://doi.org/10.1556/1886.2024.00035.
[52] Clinical and Laboratory Standards Institute (CLSI), Performance Standards for Antimicrobial Disk Susceptibility Tests; Approved Standard, Eleventh edition, 2012.
[53] A. Uberoi, A. McCready-Vangi, E.A. Grice, The wound microbiota: microbial mechanisms of impaired wound healing and infection, Nat. Rev. Microbiol. 22 (2024) 507–521, https://doi.org/10.1038/s41579-024-01035-z.
[54] WMA - The World Medical Association-WMA Declaration of Helsinki – Ethical Principles for Medical Research Involving Human Subjects, (n.d.). https://www.wma.net/policies-post/wma-declaration-of-helsinki-ethical-principles-for-medical-research-involving-human-subjects/ (accessed June 7, 2024).
[55] C.-E. Brunchi, S. Morariu, M. Bercea, Impact of ethanol addition on the behaviour of xanthan gum in aqueous media, Food Hydrocoll. 120 (2021) 106928, https://doi.org/10.1016/j.foodhyd.2021.106928.
[56] G. Horvat, M. Pantić, Ž. Knez, Z. Novak, A brief evaluation of pore structure determination for bioaerogels, Gels 8 (2022) 438, https://doi.org/10.3390/gels8070438.
[57] Y. Wang, F. Li, J. Xin, J. Xu, G. Yu, Q. Shi, Mesoporous drug delivery system: from physical properties of drug in solid state to controlled release, Molecules 28 (2023) 3406, https://doi.org/10.3390/molecules28083406.
[58] F.K. Alanazi, Utilization of date syrup as a tablet binder, comparative study, Saudi Pharm. J. 18 (2010) 81–89, https://doi.org/10.1016/j.jsps.2010.02.003.
[59] N.N. Amerhaider Nuar, S.N.A.Md. Jamil, F. Li, I.D. Mat Azmi, P.-C. Chiang, T.S. Y. Choong, Synthesis of controlled-release calcium peroxide nanoparticles coated with dextran for removal of doxycycline from aqueous system, Polymers 14 (2022) 3866, https://doi.org/10.3390/polym14183866.
[60] A. Pawlicka, F.C. Tavares, D.S. Dörr, C.M. Cholant, F. Ely, M.J.L. Santos, C. O. Avellaneda, Dielectric behavior and FTIR studies of xanthan gum-based solid polymer electrolytes, Electrochim. Acta 305 (2019) 232–239, https://doi.org/10.1016/j.electacta.2019.03.055.
[61] S. Yang, R. Chen, P. Zhang, M. Yuan, H. Li, D. Jiang, Fabrication and characterization of poly(lactic acid-trimethylene carbonate) based biodegradable composite films, Int. J. Biol. Macromol. 262 (2024) 130148, https://doi.org/10.1016/j.ijbiomac.2024.130148.
[62] P. Calza, E. Pelizzetti, M. Brussino, C. Baiocchi, Ion trap tandem mass spectrometry study of dexamethasone transformation products on light activated TiO2 surface, J. Am. Soc. Mass Spectrom. 12 (2001) 1286–1295, https://doi.org/10.1016/S1044-0305(01)00319-1.
[63] D. Ke, C. Kengla, S.J. Lee, J.J. Yoo, X. Zhu, S.V. Murphy, Release kinetics and in vitro characterization of sodium Percarbonate and calcium peroxide to oxygenate bioprinted tissue models, Int. J. Mol. Sci. 23 (2022) 6842, https://doi.org/10.3390/ijms23126842.
[64] P. George, Reaction between catalase and hydrogen peroxide, Nature 160 (1947) 41–43, https://doi.org/10.1038/160041a0.
[65] Y.-H. Lai, S. Roy Barman, A. Ganguly, A. Pal, J.-H. Yu, S.-H. Chou, E.-W. Huang, Z.-H. Lin, S.-Y. Chen, Oxygen-producing composite dressing activated by photothermal and piezoelectric effects for accelerated healing of infected wounds, Chem. Eng. J. 476 (2023) 146744, https://doi.org/10.1016/j.cej.2023.146744.
[66] A. Kumar, K.M. Rao, S.S. Han, Application of xanthan gum as polysaccharide in tissue engineering: a review, Carbohydr. Polym. 180 (2018) 128–144, https://doi.org/10.1016/j.carbpol.2017.10.009.
[67] P.L. Ritger, N.A. Peppas, A simple equation for description of solute release I. Fickian and non-fickian release from non-swellable devices in the form of slabs, spheres, cylinders or discs, J. Control. Release 5 (1987) 23–36, https://doi.org/10.1016/0168-3659(87)90034-4.
[68] S. Alfei, G.C. Schito, A.M. Schito, G. Zuccari, Reactive oxygen species (ROS)-mediated antibacterial oxidative therapies: available methods to generate ROS and a novel option proposal, Int. J. Mol. Sci. 25 (2024) 7182, https://doi.org/10.3390/ijms25137182.
[69] A. Iglesias-Mejuto, B. Magariños, T. Ferreira-Gonçalves, R. Starbird-Pérez, C. Álvarez-Lorenzo, C.P. Reis, I. Ardao, C.A. García-González, Vancomycin-loaded methylcellulose aerogel scaffolds for advanced bone tissue engineering, Carbohydr. Polym. 324 (2024) 121536, https://doi.org/10.1016/j.carbpol.2023.121536.
[70] S. Jindal, K. Ghosal, B. Khamaisi, N. Kana'an, E. Nassar-Marjiya, S. Farah, Facile green synthesis of Zingerone based tissue-like biodegradable polyester with shape-memory features for regenerative medicine, Adv. Funct. Mater. 34 (2024) 2405827, https://doi.org/10.1002/adfm.202405827.
[71] M. Weber, H. Steinle, S. Golombek, L. Hann, C. Schlensak, H.P. Wendel, M. Avci-Adali, Blood-contacting biomaterials: in vitro evaluation of the hemocompatibility, Front. Bioeng. Biotechnol. 6 (2018), https://doi.org/10.3389/fbioe.2018.00099.
[72] D. Zhang, Z. Hu, R. Hao, Q. Ouyang, C. Wang, Q. Hu, H. Li, S. Li, C. Zhu, Fabrication and hemostasis evaluation of a carboxymethyl chitosan/sodium alginate/*Resina Draconis* composite sponge, Int. J. Biol. Macromol. 274 (2024) 133265, https://doi.org/10.1016/j.ijbiomac.2024.133265.
[73] J. Tong, Q.N.Q. Vo, X. He, H. Liu, H. Zhou, C.H. Park, Physically crosslinked chitosan/αβ–glycerophosphate hydrogels enhanced by surface-modified cyclodextrin: an efficient strategy for controlled drug release, Int. J. Biol. Macromol. 283 (2024) 137163, https://doi.org/10.1016/j.ijbiomac.2024.137163.
[74] A. Iglesias-Mejuto, N. Malandain, T. Ferreira-Gonçalves, I. Ardao, C.P. Reis, A. Laromaine, A. Roig, C.A. García-González, Cellulose-in-cellulose 3D-printed bioaerogels for bone tissue engineering, Cellulose 31 (2024) 515–534, https://doi.org/10.1007/s10570-023-05601-1.